User-friendly Nonlinear Nonparametric Estimation Framework for Vibro-acoustic Industrial Measurements with Multiple Inputs

Péter Zoltán Csurcsia[a,b], Bart Peeters[a], Johan Schoukens[b]

a) Siemens Industry Software NV., Interleuvenlaan 68, 3001 Leuven, Belgium
b) Vrije Universiteit Brussel, Department of Engineering Technology, Pleinlaan 2, B-1050 Elsene, Belgium

Abstract: This paper introduces a user-friendly estimation framework for industrial measurements of vibro-acoustic systems with multiple inputs. Many mechanical structures are inherently nonlinear and there is no unique solution for modeling nonlinear systems. This is especially true when multiple-input, multiple-output (MIMO) systems are considered. This paper addresses the questions related to the user-friendly semi-automatic processing of MIMO measurements with respect to the design of experiment and the analysis of the measured data. When the proposed framework is used, with a minimal user interaction, it is easily possible a) to decide, if the underlying system is linear or not, b) to decide if the linear framework is still accurate (safe) enough to be used, and c) to tell the inexperienced (non-expert) user how much can be gained using an advanced nonlinear framework. The proposed nonparametric industrial framework is illustrated on various real-life measurements.

Keywords: MIMO systems, nonparametric estimation, nonlinear system identification, user-friendly methods, automatic processing, data segmentation, transient elimination, direct field acoustic excitation, ground vibration testing

1. Introduction

This paper presents a user-friendly semi-automatic nonparametric nonlinear industrial estimation framework of vibro-acoustic measurements with multiple inputs. Many mechanical and civil structures are inherently nonlinear. The problem related to nonlinear system identification lies in the fact that there are many different types of nonlinear systems, each of them behaves differently, therefore modeling is very involved, and universally usable design and modeling tools are not available. As coping with nonlinear systems becomes increasingly important, numerous system identification methods have been proposed. A detailed overview of the nonlinear system identification issues and challenges can be found in [1] [2] [3] and [4].

Vibro-acoustic measurements are the results of vibration testing (structural dynamic testing) techniques. Vibration testing takes place (typically) at the end of the development process and it requires a physical prototype. There is a very high time pressure due to limited availability of the fully assembled physical prototypes, and due to the tight deadline of the production date. On the other hand, the vibration testing methods are very important because they help to improve the product quality and to avoid safety and comfort issues. The goal of the vibration testing is to obtain experimental data of the whole vibrating structure such as road and air vehicles. Using these data, it is possible to validate and improve the dynamic models of systems under test.

The increasing needs for higher accuracy and faster testing techniques inspirited a lot of international researches [5] [6] [7]. As a result, time-consuming testing procedures, for instance, phase resonance method ([8] [9] [10]) are nowadays almost fully substituted by so-called phase separation techniques that find the modes by evaluating the frequency response functions (FRFs). Since the development of advanced digital signal processing algorithms and the increased computational capability, it became possible to use complex input signals such that a large variety of excitation signals can be used to experimentally determine the broadband FRFs, which are required to obtain parametric models (e.g. resonance frequencies, modes shapes in modal analysis, or e.g. state-space models in control engineering). One of the (best) possibilities is the usage of special multisines (known as pseudo random signal as well) because they can avoid spectral leakage, inconsistency, non-persistency, and they provide a handy, robust solution to build linear models (FRFs) and to detect the level and type of nonlinearities.

For complexity reasons the nonlinear systems are often approximated with linear systems, because its theory is well understood. In this work a user-friendly industrial framework is proposed to guide the users (industrial practitioners) using classical instrumentation setups, well-understood notions.

The state-of-the-art knowledge known as the Best Linear Approximation (BLA) is already available for single-input, single-output (SISO) systems [11] [12] [13] [14] [15].When a SISO system is excited by a special multisine (also known as pseudo random noise) excitation, it is possible to decide whether a linear model is still accurate enough to be used, or a nonlinear framework needs to be used. However, for multiple-input, multiple-output (MIMO) systems, the design of experiment is not a trivial question since the input and output channels are not mutually independent. Some results are already available on the design of excitation of MIMO systems [16] [17] verified on simulations only. A further requirement is that the experiment used to analyze the nonlinear behavior of the underlying system should be used to build a MIMO BLA model as well. [18] proposes a possible solution for MIMO systems with 2 inputs and 2 outputs. [16] proposes a design of experiment for MIMO systems with an arbitrary large number of input and output channels, but as was pointed out by [18], the procedure does not allow to measure the covariance matrix of the stochastic nonlinearities in the BLA setup (elaborated in detail later on). This work extends the BLA methodology to multiple-input, multiple-output (MIMO) systems with a large number of input and output channels and using orthogonal multisines (defined later on) the proposed method allows to estimate the covariance matrix of the stochastic nonlinearities in the BLA setup.

At the moment the SISO BLA evaluation process can be done by manually analyzing the FRF. The issue is that the necessary time needed to analyze the available FRFs in MIMO setup grows with the number of input and output channels, and it requires an expert user.

To overcome the above-mentioned issues, an advanced design of experiment, and a semi-automatic processing of the data are needed in order to reduce the user interactions from a few days needed to evaluate manually hundreds of transfer functions to couple of minutes. The key idea is to use a complex nonparametric estimation framework which provides a user-friendly interpretation of the measurement data by extracting the user relevant information. It interacts with the user only, if an automatic decision cannot be done and it addresses basically three fundamental questions:

1) Is the underlying system linear?

Basically, this can be done by using a special multisine (pseudo random noise) excitation. The framework (semi-automatically) analyzes the measurements and provides the user with a summary about the measurements, among other, the level and the types of nonlinearities.

2) If the system is nonlinear, are linear models still safe enough to be used?

Based on the previously mentioned information, it can also be decided whether a linear approximation can be safely used. The answer clearly depends on the required accuracy of the target application. It is possible to assign different accuracy levels (i.e. profiles) for different target applications.

3) How much can be gained using an advanced nonlinear model?

In practice, most engineers are prone to neglect the nonlinear behavior of systems because the cost of nonlinear modeling is very high. It would be beneficial to know how much can be gained by using an advanced nonlinear modeling technique instead of a linear one in order to make a well-balanced decision. The MIMO BLA model, the nonlinear distortion and noise levels will be important at this step, because the user needs to decide – based on the suggestions of the automated processing methodology– whether a simple LTI model, a BLA model, or an advanced nonlinear modeling technique is needed. The gap between the BLA errors and the noise floor of the data gives an indication of the potential gain.

Further novelties of the proposed automated methodology, for instance, highlighting strategic information, such as sensory faults during the measurement, automatic transient estimation, warning if the inputs are correlated and checks if different quantities are consistent.

Furthermore, an automatic measurement segmentation process is suggested to find back periodicity information from raw measurements. [19] provides a frequency domain an automated methodology for SISO data segmentation. In this work a fully time domain methodology is developed for MIMO measurements.

Each aspect of the proposed nonparametric industrial methodology is illustrated on real-life measurements.

This paper is organized as follows. Section 2 briefly describes the considered systems and assumptions applied in this work. Section 3 introduces the main components of the framework which are detailed in the subsequent sections. Section 4 addresses questions related to the experiment design. Section 5 provides the preprocessing and parameter setting methods. Section 6 introduces the Best Linear Approximation method and it discusses the estimation process in detail. Section 7 provides the post-processing and evaluation module of the proposed framework. Section 8 provides two measurement examples: a ground vibration testing of a small aircraft, and an acoustic test of a satellite. Conclusions can be found in Section 9.

2. Basics

2.1. Definitions and assumptions

Several definitions and assumptions must be addressed prior to carrying out any system identification procedure.

The considered systems are dynamic vibro-acoustic systems: mechanical, civil structures, passive electronics with arbitrary number of input and output channels.

The dynamics of a linear MIMO system can be nonparametrically characterized in the frequency domain by its Frequency Response Matrix (FRM, a matrix whose elements are FRFs) [20] G at frequency index k, which relates n_i inputs U to n_o outputs Y of N measurement samples as follows:

$$Y[k] = G[k]U[k] \quad (1)$$

where $G[k] \in \mathbb{C}^{n_i \times n_o}$, $Y[k] \in \mathbb{C}^{n_o}$, $U[k] \in \mathbb{C}^{n_i}$, $k = 0 \ldots \frac{N-1}{2}$ at frequency $f_k = kf_s/N$ (with sampling frequency of f_s).

In this work an arbitrary number of input and output channels are considered, and the underlying systems are casual, BIBO (bounded-input, bounded-output) stable [7] and damped systems [21].

For the sake of simplicity, the frequency indices will be omitted, and it is assumed to understand each quantity at frequency index k.

The steady-state system represented by the G is linear when the superposition principle is satisfied, i.e.:

$$Y = G(a+b)U = a\,GU + b\,GU = (a+b)\,GU \quad (2)$$

where a and b are real scalar values. When G is constant, for any a, b (and excitation), the system is called linear-time invariant (LTI). On the other hand, when G varies with a and b (and the variation depends also on the nature of excitation signal – e.g. level of excitation, distribution, etc.), the system is called nonlinear.

Further, it is assumed that the output Y is measured with additive, independent and identically distributed Gaussian noise with zero mean and finite variance σ_y (denoted as E), such that the measurement $Y_{measured}$ is given by:

$$Y_{measured} = Y + E = GU + E \quad (3)$$

It is important to highlight that the proposed framework is not limited to measurements in steady-state, and it can contain transient response (denoted as T) such that the measurement $Y_{measured}$ is given by:

$$Y_{measured} = Y + E + T = GU + E + T \quad (4)$$

In the proposed framework the input signal is measured, and it is assumed that the SNR with respect to one measurement period (block) is at least $20\ dB$. Note, that most of the mechanical and electrical measurements have a much better SNR, typically well above $40\ dB$.

Because time-varying systems are often misinterpreted as nonlinear systems, it is important to mention that when G varies over the measurement time, but at each time instant the principle of superposition is satisfied, then the system is called linear time-varying (LTV). A practical method to distinguish time-variations from nonlinearities can be found in [22].

In this work the considered systems are weakly nonlinear time-invariant systems where the linear response of the system is still present and the output of the underlying system has the same period as the excitation signal (i.e. the system has PISPO behavior: period in, same period out [23]).

2.2. Measurement setup and instrumentation

The proposed framework makes use of the classical instrumentation and measurement setups [24]. Because the interested readers of this journal come from different communities (e.g. mechanical engineering, control engineering, modal analysis, etc.) in this section the main notions used during the measurement and estimation process are defined. A general overview can be found in Fig 1, and a specific illustration on a car frame testing is shown in Fig 2.

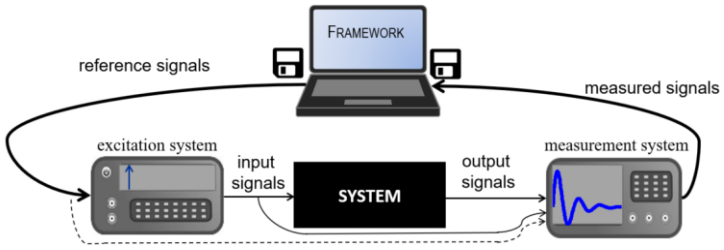

Fig 1. Theoretical schematic of the measurement-instrumentation setup. The reference signals are generated by the proposed framework, stored on the computer. The reference signals are fed to the excitation system which generates the input signals. The reference, input, and output signals are measured and stored on the computer. The dashed line highlights the fact that the reference signals are usually not measured, but it is recommended to measure or at least store these quantities. The disc symbol refers to the storage of the corresponding signals.

The reference signals are the ideal signals generated by the software framework to excite the system to be tested. In this work these signals are multisine (pseudo-random noise) signals. The excitation system (actuator) receives the (ideal) reference signal and it generates input signals to the system. In the measurement example the reference signals are the voltage signals being fed to the shakers via power amplifiers which represent the excitation system. The shakers start to move and generate forces which are the input signals to the car frame (i.e. the system under test). The output signals contain the waveforms of the system's reaction to the input signals, and they are measured with a device. In this illustration the output signals are the acceleration signals.

From instrumentation point of view, it is assumed that the measurement is perfectly synchronized i.e. samples at different channels (input and output nodes) are acquired at the same time instant, the sampling frequency is kept constant.

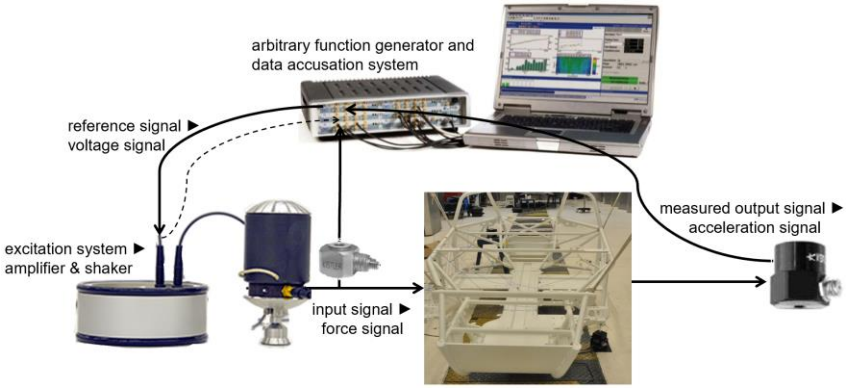

Fig 2. An illustration of the measurement-instrumentation setup used for vibration testing of the Siemens Simrod vehicle.

It is important to stress that in practice the reference signals are rarely measured or stored, and that in many cases the time-domain measurements are discarded once the FRF estimations are available. The proposed framework requires the measured time domain signals to be stored.
In the classical measurement techniques, it is almost always a silent assumption that the excitation system (actuator) is linear. However, this assumption is not guaranteed to be satisfied, and this framework is suitable to check whether the linearity assumption is fulfilled or not by measuring the reference and the input signals. If the actuator has imperfections due to its own (weak)-nonlinearities or interaction with a nonlinear system, it is possible to correct the output measurements in order to provide a better model and assessment.

3. The proposed estimation framework

Most mechanical and civil structures are nonlinear and there is no unique solution for modeling nonlinear systems. Moreover, the modeling is very involved and universally usable design tools are not available. According to the best practices of Best Linear Approximation (BLA) in SISO setup, the classical nonparametric FRF estimation procedure consists of two main steps: In the design of experiment step (step 1), the system is excited by multisine signals. Such a signal can be generated either by implementation (see later on) or by the use of toolboxes such as [25] [26].
The analysis of the measured signals (step 2) differs from the classical H1 FRF estimation process [20]. In short, H1 estimation assumes output only noise (the base-line model defined in (3)) and its value is obtained by multiplying the input auto-power input-output cross-power estimate with the inverse of the input auto-power estimate.
The key idea in the proposed approach is to make use of some statistical properties of the excitation signal such that is becomes possible to virtually split up the classical coherence function of the FRF measurement into noise and nonlinearity information. The (non)linearity assessment is based on the manual analysis of the FRF, noise and nonlinearity estimates. However, for multiple-input, multiple-output (MIMO) systems, the design of experiment is more involved, and the necessary time which is needed to analyze the available FRFs grows with the number of input and output channels. Further, to properly analyze the estimation results and to troubleshoot an experienced user is needed.
To overcome the above-mentioned issues, an estimation framework is proposed which provides a user-friendly interpretation of the nonlinear MIMO measurement data by extracting the user relevant information. This framework addresses the questions related to the semi-automatic processing of MIMO measurements with respect to the whole process. An overview of the estimation framework can be seen in Fig 3. The proposed framework consists of four interrelated steps. Next, each element of the estimation framework will be briefly discussed and later explained in detail in the following sections.

- Step 1: The *Design of experiment* and *measurement* blocks address the issues related to signal design, choice of measurement parameters, instrumentation and execution of the measurement.
- Step 2: The *Pre-processing* block considers a check-up of the input (reference) channels and provides an early warning to the user when the inputs are correlated. Furthermore, it segments the measurement data and sets up the processing parameters for the BLA transfer function estimation.
- Step 3: The *BLA estimation* block provides the BLA FRF estimation, calculates advanced statistics of the noise and nonlinearity, and when it applies estimates the transient term.
- Step 4: The *Post-processing* block makes the estimation results and warnings accessible in a condensed form. It provides users with the FRF, noise and nonlinearity estimates. It is possible to automatically highlight the FRF (or input, output, reference) channels that have significant nonlinearity or noise levels. Furthermore, channels with sensory faults and/or imperfections, and correlated inputs are detected as well.

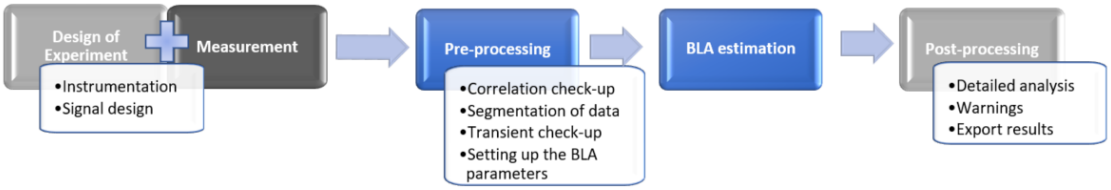

Fig 3. Overview of the proposed estimation framework. Blue blocks require – in normal circumstances – no user interactions. Light gray blocks require moderate user interaction. Dark gray block requires experienced user interaction.

The proposed estimation framework is a result of an industrial research program and at its present state it has been implemented as a combination of Simcenter Testlab [26] and Matlab components. Due to the general nature of the analysis and it can be implemented platform independently. The work has been tested with simulations and real-life industrial measurements. The warning-notification system is developed by experiences learned from typical mistakes which popped up during the measurement campaigns.

4. Design of experiment

4.1. Multisine excitation

In modern system identification special excitation signals are available to assess the underlying systems in a user-friendly, time efficient way [27]. To avoid any spectrum leakage, to reach full nonparametric characterization of the noise, and to be able to detect nonlinearities, a periodic signal is needed. Many users prefer noise excitations, because they seem simple to implement and randomness is usually needed to fulfill assumptions on estimation theories, but in this case the nonlinearities are not identifiable, and there is a possible leakage error. Using multiple levels of noise excitation allow us to detect some sort of nonlinearities, but the detailed nonlinearity assessment and classification, for a given excitation level, is not possible.
The best signal that satisfies the desired properties is the easy to implement and apply (random phase) multisine signal (see Fig 4) which looks like white noise, behaves like it but it is not a noise.
The random phase (uniformly distributed) multisine is a sum of harmonically related sinusoids. In this work, random phase multisines are used and generated in the frequency domain such that the magnitude characteristic is set by the user, the phases of the cosines are chosen randomly from a uniform distribution [23], and defined as follows:

$$u(t) = \sum_{m=1}^{F} a_m \cos(\omega_1 m t + \varphi_m),\ \varphi_m \sim \mathcal{U}(0,2\pi) \quad (5)$$

where ω_1 is the fundamental angular frequency (that sets the frequency resolution), a_m is the amplitude of the m^{th}harmonic (i.e. frequency index k) and F is the highest harmonic component.
The time-domain amplitude distribution of a random phase multisine is approximately normal: it approaches a Gaussian distribution as the number of harmonics tend to infinity. For a detailed overview of possible excitation signals we refer to [20] [24].
If the multisine contains all/only odd or even harmonics, then it is called full/odd or even multisine. Note that this signal is also known as a pseudo-random noise signal.

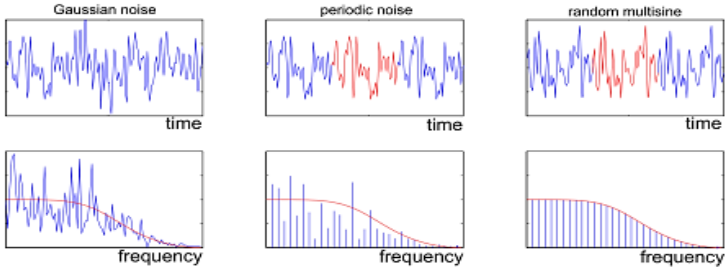

Fig 4. Different excitation signals in time and in frequency domain

4.2. Measurement illustration

This subsection illustrates the advantages of multisines on a measurement of a tire suspension system (see Fig 5). The excitation system is a hydraulic shaker which vertically moves the plate on which the tire is located. The transfer function is estimated between the force generated by the vertical displacement of the plate and one of the most dominant vertical acceleration sensors on the tire. The measurement setup and instrumentation are detailed in [28]. The system was excited by a sine sweep and multisines. The sine sweep took more than 3 minutes to measure. The multisine signal took less than 1 minute to measure. As can be seen in Fig 5, the FRF estimates are similar to each other, but the coherence function estimates differ a lot. The coherence function estimate of the multisine FRF is significantly improved. It is interesting to mention that for the multisine coherence function estimate to reach the level of coherence function estimate of the sine sweep measurement only 18 seconds were needed. The nonlinear analysis of the shaker is shown in Section 6.7.

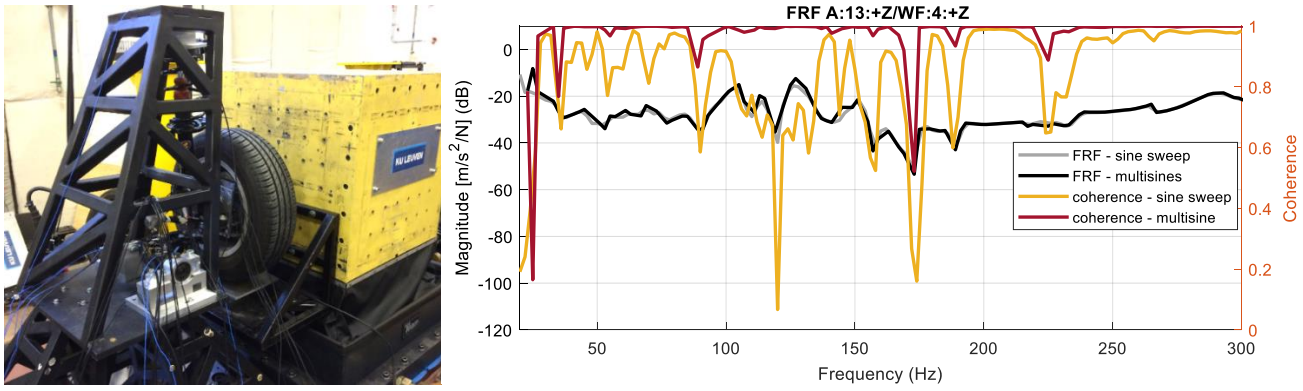

Fig 5. FRF estimation of a tire suspension measurement. On the left the measurement setup is shown. On the right the most significant FRF and coherence function estimates are shown for sine sweep and multisine excitation, respectively.

4.3. Multisines for nonlinearity evaluation

In general, when a small excitation level is used, the effects of nonlinearities can be hidden in the noise. If the excitation level is higher, the effect of the nonlinearities become visible. If a full-band multisine excitation is used, then the details of the nonlinear behavior are not directly separable from the linear part. Fig 6 shows an example, how the system response consists of the linear and nonlinear part. When an excitation set of only even harmonics is used, the odd nonlinearities are not detectable. The solution to detect both even and odd nonlinear contributions is to use an excitation set only with odd harmonics, e.g. odd random phase multisine. In order to examine the odd frequencies, it is needed to skip several odd harmonics in the multisine. The experiences show that the odd, random phase multisine with randomly skipped harmonics is the best what can be used because when a fixed odd harmonic is missing then certain type of nonlinearities can be hidden. A random skipping is recommended to be done within a fixed group of harmonics (F_{group}). The authors recommend using a group of three or four, i.e. in each series of three/four odd harmonics, one odd harmonic is skipped randomly. The disadvantage of the missing harmonics multisine is that the effective frequency resolution becomes coarser, but on the other hand, at the same power level of the excitation system, the frequency components can be more excited. A further advantage is to mention that using band-limited multisines allows the user to detect in-band and out-band nonlinearities, i.e. to detect that the nonlinearities are limited to the band of excitation or not.

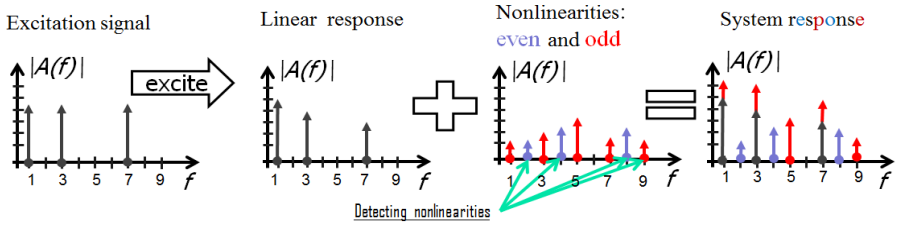

Fig 6. System response originating from linear and nonlinear part of excited system

4.4. Multisines for multiple input measurements

When considering a MIMO measurement setup, it seems to be handy to excite each of the input separately. This technique raises some important questions. First, the principle of superposition is only valid for linear systems. Second, in this case, significantly more experiments are needed which drastically increases the time needed to measure and analyze the FRFs. Therefore, a more advanced measurement procedure is advised. For the sake of simplicity – without loss of generality – we will focus on systems with three inputs and two outputs, a block illustration of such a setup is shown in Fig 7. This allows to illustrate the additional problems that appear when moving from SISO to MIMO for a minimal increase of the complexity.

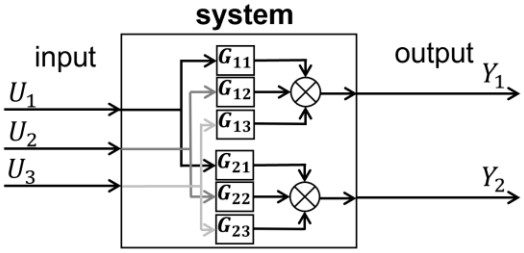

Fig 7. Illustration of a system with three inputs and two outputs.

The straightforward extension of the SISO excitation case can be formulated in the frequency domain at the excited frequency bins (lines) as follows:

$$Y = GU \Leftrightarrow \begin{bmatrix} Y_1 \\ Y_2 \end{bmatrix} = \begin{bmatrix} \mathrm{G}_{11} & \mathrm{G}_{12} & \mathrm{G}_{13} \\ \mathrm{G}_{21} & \mathrm{G}_{22} & \mathrm{G}_{23} \end{bmatrix} \begin{bmatrix} U_1 \\ U_2 \\ U_3 \end{bmatrix} \tag{6}$$

where the indices of the input and output data refer to channel number.
Even when there are multiple periods of excitation applied, the above-mentioned set of linear equations suffers from the degrees of freedom: there are 6 unknown parameters and only 2 independent equations (in other words there is a rank deficiency). In order to overcome the issue with the degrees of freedom, then number of independent equations must be increased. In this work this has been done by increasing the number of experiments by expanding the number of columns in *U* (and hence the number of columns in *Y*). Each column in *U* (*Y*) represents an experiment. In case of 3 inputs there are at least 3 experiments needed such that the new base-line equation is defined as follows:

$$\begin{bmatrix} Y_{[1,1]} & Y_{[1,2]} & Y_{[1,3]} \\ Y_{[2,1]} & Y_{[2,2]} & Y_{[2,3]} \end{bmatrix} = \begin{bmatrix} G_{11} & G_{12} & G_{13} \\ G_{21} & G_{22} & G_{23} \end{bmatrix} \begin{bmatrix} U_{[1,1]} & U_{[1,2]} & U_{[1,3]} \\ U_{[2,1]} & U_{[2,2]} & U_{[2,3]} \\ U_{[3,1]} & U_{[3,2]} & U_{[3,3]} \end{bmatrix} \tag{7}$$

where the first digit of the indices in square brackets refers to channel and the second digit refers to the number of experiment. To obtain the FRM estimate, at each excited frequency index (7) must be solved.

The solvability of the above-mentioned linear algebraic equation strongly depends on the condition number (i.e. the randomness) of the excitation signal matrix *U*. In classical MIMO identification, one of the most often applied solution to this problem is the use of Hadamard decorrelation technique (known as +- technique as well [29]: a square matrix (whose entries are either +1 or −1) is elementwise multiplied with one single realization of the signal. The restriction is that the order of the Hadamard matrix must be 1, 2, or multiples of 4. For input dimensions where the Hadamard matrices cannot be defined, the most often used solution is to take the Hadamard matrix with highest closest order and truncate it to the desired size: the necessary matrix is cut out from the upper left region of the Hadamard matrix. In this section there are 3 inputs considered. The closes Hadamard order is 4:

$$\begin{bmatrix} +1 & +1 & +1 & +1 \\ +1 & -1 & +1 & -1 \\ +1 & +1 & -1 & -1 \\ +1 & -1 & -1 & +1 \end{bmatrix} \tag{8}$$

From here the upper left square 3x3 matrix has to be used such that the excitation signal is given by:

$$U_{Hadamard} = \begin{bmatrix} U_1 & U_1 & U_1 \\ U_1 & -U_1 & U_1 \\ U_1 & U_1 & -U_1 \end{bmatrix} \tag{9}$$

For certain dimensions this solution might be not adequate and rich enough to identify the nonlinearities because only one realization of the input signal is applied (for detecting the nonlinearities richer signals are required). Further, it is very important to highlight that a measurement using Hadamard structure unnecessarily "stretches" the structure. For example, think of the vibration testing of a symmetric structure, for instance, an airplane where the wings are excited. The "stretch" appears by applying inputs of opposite sign at certain time instances.

In order to overcome the issue with the limited possible orders of Hadamard matrix and to improve the estimation properties [30] and [31] proposed to use orthogonal random multisines, extending the idea of the orthogonal inputs proposed for linear MIMO measurements in [32]. In this work the proposed procedure is to generate independent random excitation for every input channel such that we have (more) randomness in the measurement with respect to the Hadamard's technique. This sequence of signals will be placed in the first blocks of experiments (i.e. first column of *U*) and they will be orthogonally phase shifted for the subsequent experiments (i.e. the next columns in *U*) with the weighting matrix *W* having the following elements:

$$W_{cn} = e^{-\frac{j2\pi(c-1)(n-1)}{n_i}} \tag{10}$$

where $W \in \mathbb{C}^{n_i \times n_i}$, *c* refers to input channel number (i.e. the row number in *U*), *n* refers to the experiment number (column number in *U*), and n_i stands for the number of inputs. In case of 3 input channels the following equation is given:

$$W = \begin{bmatrix} 1 & 1 & 1 \\ 1 & e^{-\frac{j2\pi}{3}} & e^{-\frac{j4\pi}{3}} \\ 1 & e^{-\frac{j4\pi}{3}} & e^{-\frac{j8\pi}{3}} \end{bmatrix} = \begin{bmatrix} 1 & 1 & 1 \\ 1 & e^{-\frac{j2\pi}{3}} & e^{\frac{j2\pi}{3}} \\ 1 & e^{\frac{j2\pi}{3}} & e^{-\frac{j2\pi}{3}} \end{bmatrix} \tag{11}$$

such that the excitation matrix is given by – with elementwise multiplication $\odot$:

$$U_{ms} = U \odot \mathrm{W} = \begin{bmatrix} U_1 & U_1 & U_1 \\ U_2 & e^{-\frac{j2\pi}{3}}U_2 & e^{\frac{j2\pi}{3}}U_2 \\ U_3 & e^{\frac{j2\pi}{3}}U_3 & e^{-\frac{j2\pi}{3}}U_3 \end{bmatrix} \tag{12}$$

It is important to highlight that it is possible to use multiple periods (blocks) of multisines. Using multiple periods, the SNR will be improved. If there are *P* periods (blocks) applied, then the excitation signal is given by:

$$U_{ms} = \begin{bmatrix} \overbrace{U_1 \ \dots U_1}^{P-times} & \overbrace{U_1 \dots U_1}^{P-times} & \overbrace{U_1 \ \dots U_1}^{P-times} \\ \overbrace{U_2 \ \dots U_2}^{P-times} & e^{-\frac{j2\pi}{3}}\left(\overbrace{U_2 \ \dots U_2}^{P-times}\right) & e^{\frac{j2\pi}{3}}\left(\overbrace{U_2 \ \dots U_2}^{P-times}\right) \\ \overbrace{U_3 \ \dots U_3}^{P-times} & e^{\frac{j2\pi}{3}}\left(\overbrace{U_3 \ \dots U_3}^{P-times}\right) & e^{-\frac{j2\pi}{3}}\left(\overbrace{U_3 \ \dots U_3}^{P-times}\right) \end{bmatrix} \tag{13}$$

It is highly recommended to enrich the randomness of the (periodic) multisines by adding multiple random realizations, see Section 6.2 for a detailed explanation.

In case of M independent random realizations and P periods, the excitation signal is given by:

$$U_{ms} = \overbrace{\begin{bmatrix} \overbrace{U_1^{(1)} \dots U_1^{(1)}}^{P-times} & \overbrace{U_1^{(1)} \dots U_1^{(1)}}^{P-times} & \overbrace{U_1^{(1)} \dots U_1^{(1)}}^{P-times} \\ \overbrace{U_2^{(1)} \dots U_2^{(1)}}^{P-times} & e^{-\frac{j2\pi}{3}}\left(\overbrace{U_2^{(1)} \dots U_2^{(1)}}^{P-times}\right) & e^{\frac{j2\pi}{3}}\left(\overbrace{U_2^{(1)} \dots U_2^{(1)}}^{P-times}\right) \\ \overbrace{U_3^{(1)} \dots U_3^{(1)}}^{P-times} & e^{\frac{j2\pi}{3}}\left(\overbrace{U_3^{(1)} \dots U_3^{(1)}}^{P-times}\right) & e^{-\frac{j2\pi}{3}}\left(\overbrace{U_3^{(1)} \dots U_3^{(1)}}^{P-times}\right) \end{bmatrix}}^{1^{st}\ set\ of\ indepedent\ U\ signals} \dots \overbrace{\begin{bmatrix} \overbrace{U_1^{(M)} \dots U_1^{(M)}}^{P-times} & \overbrace{U_1^{(M)} \dots U_1^{(M)}}^{P-times} & \overbrace{U_1^{(M)} \dots U_1^{(M)}}^{P-times} \\ \overbrace{U_2^{(M)} \dots U_2^{(M)}}^{P-times} & e^{-\frac{-j2\pi}{3}}\left(\overbrace{U_2^{(M)} \dots U_2^{(M)}}^{P-times}\right) & e^{\frac{j2\pi}{3}}\left(\overbrace{U_2^{(M)} \dots U_2^{(M)}}^{P-times}\right) \\ \overbrace{U_3^{(M)} \dots U_3^{(M)}}^{P-times} & e^{\frac{j2\pi}{3}}\left(\overbrace{U_3^{(M)} \dots U_3^{(M)}}^{P-times}\right) & e^{-\frac{j2\pi}{3}}\left(\overbrace{U_3^{(M)} \dots U_3^{(M)}}^{P-times}\right) \end{bmatrix}}^{M^{th}\ set\ of\ indepedent\ U\ signals} \quad (14)$$

4.5. Implementation

It is assumed that the measurement and instrumentation are prepared using best practices. The instrumentation is chosen according the necessary precession of the target application, and there are no synchronization issues in the measurement system (i.e. the sampling of the input-output channels does not happen at the same time, the sampling time is not constant). Many setups require safety fade-in, fade-out segments of the measurement. It is used to allow the system to warm-up and cool-down gradually. In generally it is recommended to set these values to zero seconds such that they are not measured. If, for any reasons, it is not possible, additional periods of the excitation signal are recommended to be used at the beginning and at the end of the measurement which can be easily discarded. If, due to limited measurement time, this is not possible, the estimation framework will tackle the fade-in, fade-out data as transient. For a detailed overview related to instrumentation questions we refer to [24].

In the proposed estimation framework, it is advised to have two different parameter setting modes: the general mode and the detailed mode. The first one is intended for general applications where only a minimal amount of signal parameters are required to be defined, and most of the parameters can be automatically set, and therefore, the detailed options can be hidden. The user has to choose at least the following parameters:

- The sampling frequency (f_s), this is usually determined by the components of the instrumentation and the system under test.
- The number of input channels (n_i), determined by the system and/or experiment.
- The maximum power/amplitude level of excitation: determined by the safety margins of the system/instrumentation.
- The frequency resolution (f_{res}) or the number of samples in one period N (the relationship is $f_s = f_{res}N$).

Note, that if the target application has a standard frequency resolution (f_{res}) then it is possible to predefine this value as well. For instance, for most of the vehicle testing application $0.1 \dots 0.5\ Hz$ resolution is sufficient.

Based on the above-mentioned parameters, the rest of the options can be initialized with default values. However, in the detailed mode, for specific applications, these defaults can also be changed by the user. It concerns the following parameters:

- The lowest excited frequency component, default is f_{res}. Please note that it is not recommended to be set to $0\ Hz$ (DC component) [27].
- The highest excited frequency component, default is $0.4f_s$. It is important to mention that system theory allows a choice of $0.5f_s$ but the analogue electronics parts of the instrumentation (conditioning, anti-aliasing filters) have never ideal characteristics.
- The magnitude characteristics (a_m in (5)): a flat profile is used which is scaler to match the maximum amplitude level defined above.
- The minimum power (rms) and or amplitude level of excitation, the default is set to 10% of the maximum level
- The number of levels used for the experiment. It is recommended to use at least 2 levels of excitation: minimum, and maximum.
- The number of periods and realizations: According to the recommendations of [20] the default number of periods is three and there are seven different realizations. A discussion about the effect of number of periods/realizations can be found in Section 6.3.
- The type of harmonics excited in the band of excitation: even, odd or full. Default choice is odd (see Section 4.3).

In case of odd multisines:

- The index of the skipped harmonics is recommended to be a random number (see Section 4.3).
- The number of odd of harmonics in a group (F_{group}) where one harmonic is skipped: default is 4.

All these settings are recommended to be added as metadata to the excitation signal and stored together with the measurement files.

5. Pre-processing

5.1. Overview

After the measurement is executed, the acquired data must be pre-processed: the trends (at least the mean/offset values) must be removed [27]. Once the model is available, for simulation purposes, the simulated signals can be easily updated with the trends. The next step is the segmentation of data: retrieving the periods, realizations and phase rotations. Based on these processed segmented data an early quality assessment of experimental data is done, and the parameters for the BLA estimation procedure are set. The general process is illustrated on the flowchart shown in Fig 8. Next, the main building blocks of the process are explained.

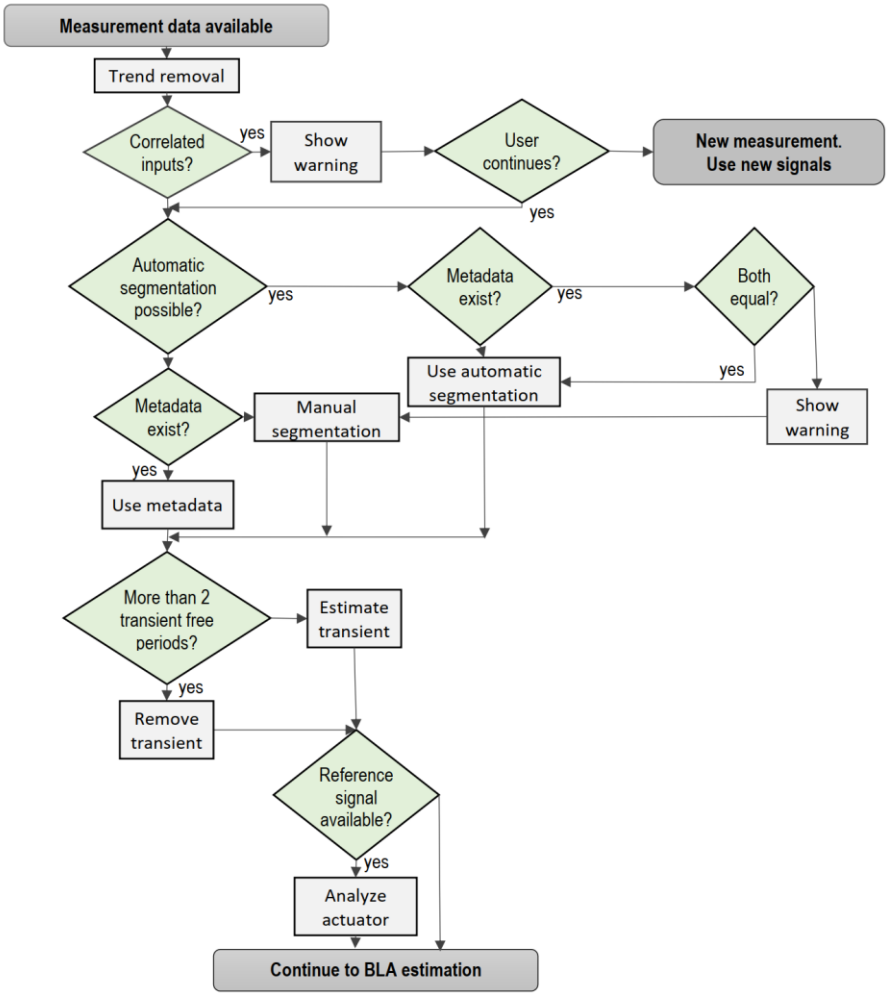

Fig 8. Flowchart of the pre-processing block.

5.2. Input correlation check-up

As explained in Section 4.4 the MIMO FRM estimation procedure ideally requires independent (uncorrelated) excitation signals. Using multiple channels, it can easily happen that by mistake two or more input channels share the same signal. If the continuation of the estimation processing happens, the user will face with low quality (noisy like) FRF estimates. Without indicating the correlation of the excitation signals, the user would have a really difficult time to debug and find out the underlying reason behind the bad quality FRM estimate.

In the proposed framework the absolute correlation coefficient ρ of the reference and/or input signals is used. It is calculated for two input channels i and j as follows (provided that 0 Hz (DC component) is not excited):

$$\rho(u_i, u_j) = \left| \frac{\sum_{k=1}^{N_{total}} u_i[k] u_j[k]}{\sqrt[2]{\sum_{k=1}^{N_{total}} u_i^2[k]} \sqrt[2]{\sum_{k=1}^{N_{total}} u_j^2[k]}} \right| \tag{15}$$

where $u_i[k]$ refers to the time-domain measurement of the input signal at channel i at time instant k, $i, j = 1 \dots n_i$, n_i is the number of input channels, N_{total} is the number of samples in the entire measurement, $\rho(u_i, u_j)$ is the $(i,j)^{th}$ element of the correlation coefficient matrix $C \in \mathbb{R}^{n_i x n_i}$, and $0 \leq \rho(u_i, u_j) \leq 1$.

The automatic processing is interrupted, and the user is warned, if any off-diagonal element of the correlation coefficient matrix C is greater or equal than the predefined threshold level $\kappa_{correlation}$ (the recommended is $\kappa_{correlation}$ is 0.8), i.e. when the following inequality is satisfied:

$$\rho(u_i, u_j) \geq \kappa_{correlation},\ i,j = 1 \dots n_i, i \neq j \tag{16}$$

It is also recommended to calculate the absolute correlation coefficient for both the reference and input signals. If the input channels are shown to be correlated but the reference channels are not, this means that there are wiring/connection issues at the actuator (excitation system). When the reference and input signals are both correlated, it is very likely the operator assigned wrong signals for the channels. In both cases a new experiment is recommended to be executed.

5.3. Data segmentation

In the ideal case metadata (the parameters given in Section 4.5) are available and can be used to segment the measured. In real-life situations, the instrumentation (measurement) systems and the software frameworks can have different file formats, and this may result in the loss of the metadata. However, in most of the cases it is possible to have automatic data segmentation based on the measurement data only. When the sampling frequency and number of input channels are pre-defined (known), a simplified statistical process can be used to retrieve the meta information.

5.3.1. Period length N

In the proposed framework this process is based on the absolute value of the one-sided biased auto-correlation estimate of the input data (reference or input signal) [33], and it is calculated at τ lag as follows:

$$\hat{R}_i[\tau] = \left| \frac{1}{N_{total}} \sum_{k=1}^{N_{total}} u_i[k] u_i[\tau + k] \right|, \quad \tau = 0 \dots N_{total} - 1 \tag{17}$$

where i stands for the i^{th} input channel, N_{total} is the total number of measurement samples.

Next, each is $\hat{R}_i$ is normalized to its maximum value such that:

$$\hat{R'}_i = \frac{\hat{R}_i}{\hat{R}_i[0]} \tag{18}$$

Based on values of $\hat{R'}_i$ a peak-position finding process must be used. If the multisine is ideally generated and measured, then the autocorrelation function should contain peaks with the distance that correspond to the length of the period (block size) N, and at any other position the autocorrelation function should be zero. Because the measured signals can contain noise, transient, nonlinearities and other disturbances, the autocorrelation function estimates will be not ideal. Therefore, it is important to parametrize the peak-position finding process. An experimental illustration can be seen in Fig 9.

It is recommended for the peak detection algorithm to use at least a height of 0.2 and minimum distance of $10/f_s$, i.e. minimum distance of ten times the sampling time. With the height parameter we make sure that only the significant components are considered. In case of mechanical systems, the applied period length is typically much larger than 0.1 second. The positions of the peaks for the concatenated autocorrelation $\hat{R}'$ function is given by

$$peak\ locations = peakdetection(\hat{R}')_{\text{Minimum height=0.2,Mininum distance=}10/f_s} \tag{19}$$

where $\hat{R}'=\{\hat{R'}_1, \dots, \hat{R'}_{n_i}\}$, and n_i is the number of inputs.

Based on (19) the potential length of the period (block) is given by the statistical mode (element with the highest occurrence) of the distance between peaks:

$$N_{est} = mode(\Delta peak\ locations) \tag{20}$$

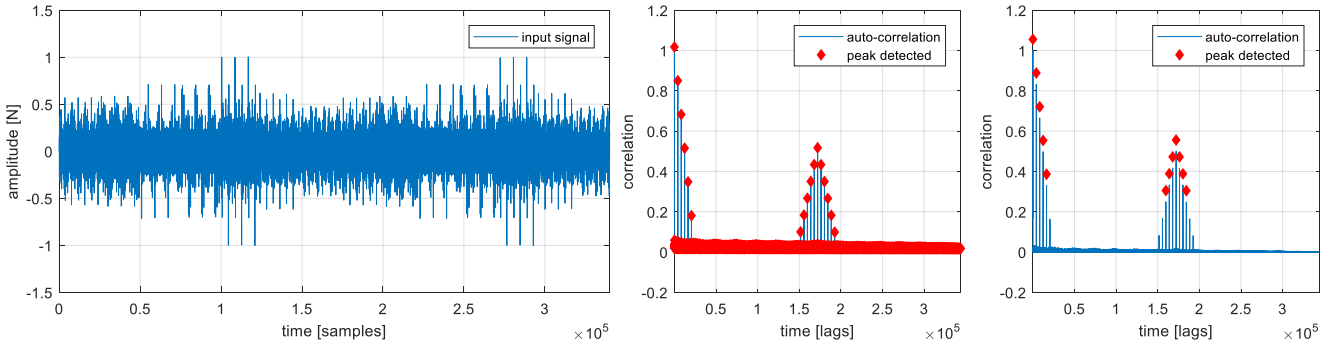

Fig 9. Autocorrelation estimates of a wind turbine blade measurement. One period (block) contains 8192 samples. There are 3 periods, 7 realizations and 2 phase rotations (for the 2 input channels). The figure left shows the raw measurement of the first input measurement channel. The middle and right figures show the autocorrelation estimates according to (17)-(18). The middle figure shows the peak detection algorithm without parametrization. The right figure shows the peak detection algorithm with parametrization.

If full-band multisines (e.g. each frequency is excited) are used, then $N = N_{est}$. If even or odd multisines are used, then $N = 2N_{est}$. If the information with respect to the type of multisines is not available, then it can be retrieved by testing the data. Assuming that there are at least two periods, it can be tested whether the input signals have N_{est} or $2N_{est}$ periodicity. $N = 2N_{est}$ (i.e. we have no full band multisines) when the following inequality is satisfied:

$$\frac{1}{n_i}\sum_{i=1}^{n_i}||u_i[1\dots 2N_{est}]-u_i[2N_{est}+1\dots 4N_{est}]||_2^2 < \frac{\kappa_{transient}}{n_i}\sum_{i=1}^{n_i}||u_i[1\dots N_{est}]-u_i[N_{est}+1\dots 2N_{est}]||_2^2 \quad (21)$$

where $||x||_2^2$ is the Frobenious norm of x and $\kappa_{transient} \in \mathbb{R}^+ < 1$ is a number used to compensate the transient effect.
In other words, we are testing that if the averaged "periodicity" error between consequent blocks of N_{est} or $2N_{est}$ is smaller. $\kappa_{transient}$ plays an important role when full-band multisines (i.e. $N = N_{est}$) and at least four periods are used. Should the measurement contain transient, the inequality (21) would be satisfied without $\kappa_{transient}$ term, because the first part of the measurement is disturbed with exponentially decaying transient. In this work, based on experience, it is suggested to set $\kappa_{transient}$ to 0.5.

5.3.2. Number of periods P

Once the length of the period (block) N is estimated, the number of periods P has to be estimated. This can be done by checking the correlation coefficient between the first and the consequent blocks of N. The number of periods P will be the furthest N segment where there if still high correlation, i.e.:

$$\frac{1}{n_i}\sum_{i=1}^{n_i}\rho\,(u_i[1\dots N];\, u_i[(p-1)N+1\dots pN]) > \kappa_{correlation} \quad (22)$$

where $p \in \mathbb{N}^+$ is largest integer number where the inequation is still true.
Please note that in (21) and (22) the overall effect of all the input (excitation) channels are used in order to overcome the unexpected effects caused by disturbances and imperfections of actuator. In other words, instead of focusing on the analysis of one channel, we focus on the overall behavior of all channels.

5.3.3. Number of realizations M

The last step in the segmentation process is to estimate the number of realizations M (i.e. number of different P blocks). The total length N_{total} contains n_i-times phase rotated M segments (see Section 4.4) and it has to be divided by n_i. The number of realizations M is then given by:

$$M = round\ down\left(\frac{round\ down\left(\frac{N_{total}}{n_i}\right)}{PN}\right) \quad (23)$$

Because it is quite common that the measurement length is a little bit longer than the length of the measurement signal N_{total} (i.e. a few extra samples are measured), the rounding function is needed to overcome possible issues and to have an integer M. The proposed segmentation method is proofed to be very robust, however, when the input signal becomes extremely distorted (due to a nonlinear excitation system) it might fail to detect the correct number of periods, this happened only in few instances (where the reference signal was not accessible, and the excitation system operated in nonlinear regime).
A mismatch between the result of the automated segmentation and meta data information can only fail (with an exception of the above-mentioned case) if the measurement is terminated earlier as planned, for instance, due to a failure in the setup.

5.4. Transient detection

For most of the nonparametric FRF estimation methods it is crucial that the steady-state signals are considered, otherwise the transient term is included in the estimated FRF model, and therefore, it will be not an adequate representation of the system. The transient term occurs when the system is initially not at rest, when the past values of the excitation signal are unknown, when there is a change in the excitation signal or when fade-in/fade-out is used.
When many periods are available, it is the best practice to discard the first few blocks (the transient periods or in other words, the delay blocks). When it is not possible, different windowing methods are used in practice [20] [24] [34]. In order to ensure that the measured signals are in the steady-state, a simple transient check-up is performed. An illustration on a battery-operated small aircraft [35] is shown on Fig 10. It shows the first realization of one of the most dominant output channels in time domain. In order to determine the length of the transient (i.e. the number of delay blocks), the last block (period) of the first realization – assumed to be (nearly) in steady-state – is subtracted from every block in that realization. As can be seen on the right side of Fig 10, only the first block is disturbed by the transient. In this case, each first period (block) is discarded.
In the proposed framework, if there are at least 3 periods (blocks) available, the length of the transient term is estimated. If, for any reasons, the transient term cannot be eliminated by chopping a (few) block(s) (e.g. there are less than 3 periods, or the transient term is very long), then it is estimated with a special direct implementation of local rational method [36], as detailed in Section 6.6.
The transient length determination algorithm takes all output channels into account. If there are multiple realizations/phase realizations of the multisine excitation, only the first one is considered. For each period the rms difference with respect to the last period (block) of the considered output channel is calculated as follows:

$$rms[i,j] = \left\|y_{i,[P]} - y_{i,[j]}\right\|_2^2, i = 1\dots n_o, j = 1\dots P-1 \quad (24)$$

where $y_{i,[j]}$ refers to the time-domain measurement of the output signal at channel i at period j, n_o is the number of outputs, $\|y\|_2^2$ refers to the Frobenois norm of y and P is number of periods.
Next, for each channel a threshold is defined as two-times the standard deviation of (24):

$$\kappa_{treshold}[i] = 2\ std\ (rms[i]) \quad (25)$$

Finally, the estimated number of transient disturbed periods (delay blocks) is then given by

$$P_{tr} = j,\ rms[i,j] \geq \kappa_{treshold}[i],\ i = 1\dots n_o \quad (26)$$

where j is the highest number where the inequality is still satisfied.
The last step is that the transient disturbed periods are discarded (in each data channel, realization, phase rotation), and P is corrected with p_{tr} (i.e. the new P is given by $P - P_{tr}$).

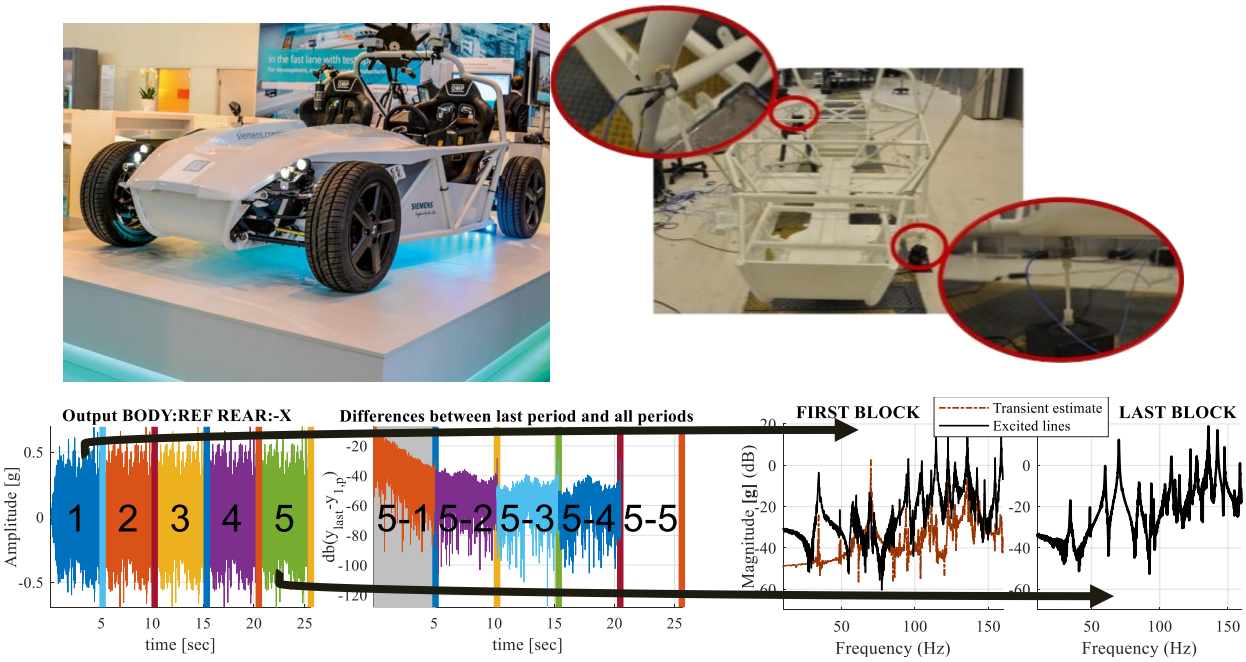

Fig 10. Periodicity check-up of a car frame measurement. The car frame is excited horizontally and vertically. The left bottom figure shows the force measurement of the block repetitions in one realization at the horizontal driving point. The second bottom figure shows the difference between the last block minus every block. The gray area refers to the automatically detected transient periods. The third and fourth bottom figures show the spectrum estimates of the first and last blocks.

5.5. Setting up parameters

The last step of the pre-processing block of the proposed framework is to choose the processing method of the FRM estimation method discussed in the next section. If there are at least three periods (block) available, then the transient check-up algorithm must be called. If there are less than three transient-free periods, then the FRM estimation is calculated with the transient estimation method as detailed in Section 6.6. Otherwise, the transient disturbed periods (blocks) are discarded and further choices are possible.
If the reference signal is available, then the BLA of the actuator is also estimated. These steps are detailed in the next section.

6. Best linear approximation

6.1. Introduction

The Best Linear Approximation (BLA) has been widely used in the last decades to efficiently estimate FRFs [27]. The BLA of a nonlinear system is a modeling approach that minimizes the mean square error between the true output of a nonlinear system and the output of the linear model. The proposed BLA technique makes use of the knowledge that the excitation signal has both stochastic and deterministic properties. In this work the excitation signal is an odd random phase multisine signal (see Section 4.1) and it is assumed to be measured precisely. In each measurement there are M different random realizations of multisines (orthogonally shifted n_i times i.e. number of input channels times) and each of the realization is repeated P times (there are P repeated blocks in each segment), see Section 4.4.
From the philosophical point of view there are two main differences between the proposed BLA and the classical H1 (product of the output-input cross spectrum matrix and the inverse of input power spectrum matrix) estimate [24] [37] frameworks. First, in the BLA case the FRM is estimated from the discrete Fourier transformed data instead of using the cross-power and auto-power matrices and it involves no windowing functions. Second, instead of directly using the averaged input and output data, a partial BLA estimate is calculated for each period (and its phase-shifted period-pairs) of the excitation. A BLA FRM estimate, for a given signal, is then calculated via the average of partial BLA estimates, see Fig 13. In this case we can easily estimate the noise levels and standard deviations on each frequency line. Using this information, the coherence function will be virtually split into (1) noise level and (2) nonlinear contribution estimates as illustrated on a ground vibration testing experiment of an F16 aircraft in Fig 11. It will be explained in the following how these results are obtained.

Please note that in case of ideally measured multisine experiments the unwindowed H1 and BLA estimation results in the same transfer function estimation, however, using H1 methodology no advanced information is made available on the noise and nonlinearities.

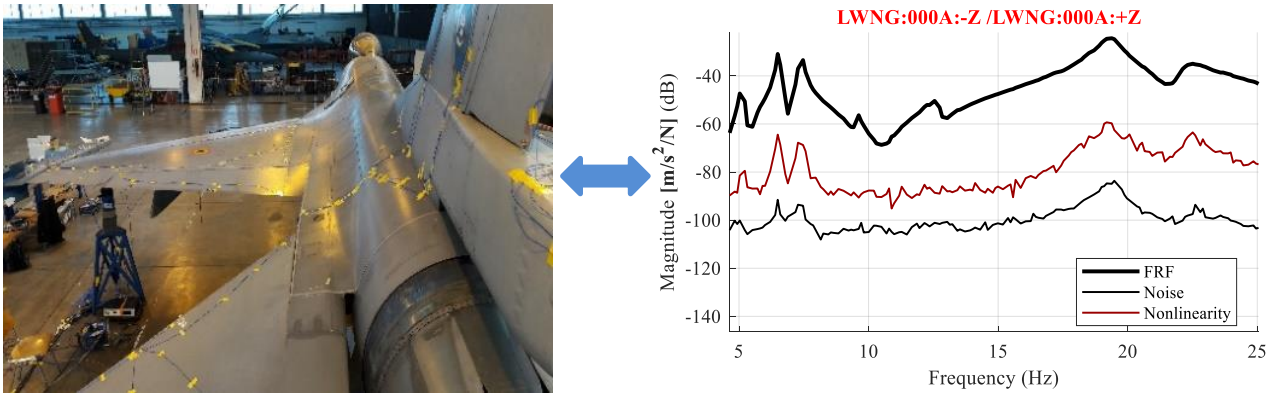

Fig 11. The best linear approximation of a ground vibration testing experiment of an F16 aircraft. The experiment is shown on the left. The results are shown on the right. The thick black line shows the FRF. The red line shows the level of nonlinear distortion and the thin black line shows the noise.

6.2. Theoretical structure and the basic assumptions

As aforementioned, the BLA of a nonlinear system is an approach of modeling that minimizes the mean square error between the true output of a nonlinear system and the output of the linear model [23]. In the proposed BLA framework, multiple repeated realizations of random phase multisine excitation are needed. The BLA estimate consists of several components. The theoretical structure of the considered BLA estimator is shown in Fig 12.

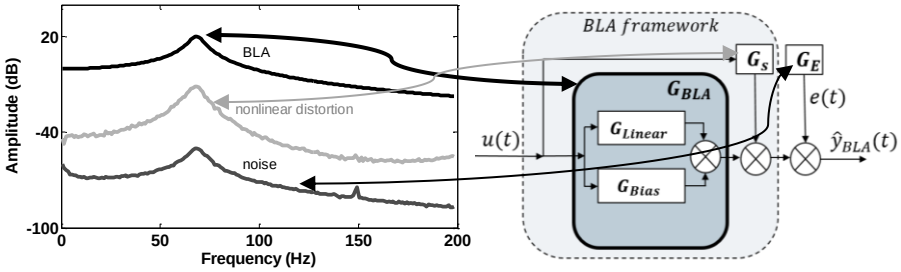

Fig 12. The theoretical structure of the best linear approximation and its connection to the FRF estimate.

$G_{Linear}$is the linear (transfer function) component of BLA. This component is phase coherent: random phase rotation in the input excitation results in a proportional phase rotation at the output.
In case of non-coherent behavior, the input phase rotation results in a random phase rotation at the output. Please note that significant part of the nonlinearities is non-coherent. When many input phase rotations are performed, the random output rotations can be seen as an additional (nonlinear) noise source (G_s) next to the ordinary measurement noise source component (G_E). The noise source component (G_s) varies only over different realizations and it is assumed to be additive i.i.d. normal distributed with zero mean with a finite variance. The generated nonlinear noise signal is denoted by signal Y_s, it is uncorrelated but dependent on the realization. The measurement noise component G_E represents an autonomous system: the output measurement error E (additive i.i.d. normal distributed with zero mean with a finite variance) is from the input independently generated. When its effect is observed on the FRF estimation E is only scaled with the input.
The usage of periodic excitation reduces the effects of the measurement noise component G_E. The usage of multiple random phase realizations reduces the impact of non-coherent nonlinearities represented by G_s on the BLA estimation.
The (coherent) nonlinearities remaining after multiple realizations of excitation signal result in a bias error of the BLA (denoted by G_{Bias}). The next section discusses a possibility to reduce the effects of G_S, G_E.

6.3. Multidimensional averaging

When the BLA estimation framework is applied, the observed system is excited by random phase multisines. In this work there are (n_i input number times phase-rotated) M different realization of the multisine excitation signal, each realization is repeated P period times. The considered steady-state model at period p and realization m at excited frequency bin k is given by as a straightforward extension of the baseline model in (3) and Fig 12:

$$Y_{measured}^{[m][p]} = Y^{[m][p]} + E = \left(\hat{G}_{BLA} + \hat{G}_S^{[m]}\right)U^{[m]} + E^{[m][p]} \quad (27)$$

such that the measured FRF is given by:

$$\hat{G}^{[m][p]} = Y_{measured}^{[m][p]} U^{[m]^{-1}} = \hat{G}_{BLA} + \hat{G}_S^{[m]} + \hat{G}_E^{[m][p]} \tag{28}$$

where $\hat{G}^{[m][p]} \in \mathbb{C}^{n_i \times n_o}$, $\hat{Y}_{measured}^{[m][p]} \in \mathbb{C}^{n_o}$, $U^{[m]} \in \mathbb{C}^{n_i}$ and the x^{-1} is the generalized (Moore–Penrose) inverse of x.

For computational optimality, it is suggested that (28) is solved output channel-wise (i.e. one output channel per time). The BLA estimate should be calculated at the excited frequency lines only. In the frequency band of excitation, the BLA estimates at the non-excited bins are obtained by linear (1st order) interpolation.

As discussed in Section 5.4, the steady state-signals either obtained by discarding some periods at the beginning of each realization block or the transient term is estimated. In order to estimate the BLA one has to average over P periods (blocks) of repeated excitation signal, and over the M different realizations of the excitation signal [23] as illustrated in Fig 13.

First, let us average over the P periods of a realization.

$$\hat{G}^{[m]} = \frac{1}{P}\sum_{i=1}^{P} \overbrace{\hat{G}^{[m][p]}}^{measured\ FRF} = \frac{1}{P}\sum_{p=1}^{P} \left(\overbrace{\hat{G}_{BLA}^{[m]}}^{\substack{FRF \\ estimate}} + \overbrace{\hat{G}_S^{[m]}}^{\substack{nonlinearity \\ fixed\ in\ m}} + \overbrace{\hat{G}_E^{[m][p]}}^{\substack{noise \\ varies\ over\ p}} \right) = \hat{G}_{BLA}^{[m]} + \hat{G}_S^{[m]} + \frac{1}{P}\sum_{i=p}^{P} \hat{G}_E^{[m][p]} = \tag{29}$$

$$\hat{G}_{BLA} + \hat{G}_S^{[m]} + \frac{1}{P}\sum_{p=1}^{P} \underbrace{E^{[m][p]}}_{\mathcal{N}(0,\sigma_y)=E^{[m]}} |U|^{-1} = \hat{G}_{BLA}^{[m]} + \hat{G}_S^{[m]} + \underbrace{\hat{G}_E^{[m]}}_{\mathcal{N}\left(0,\frac{\sigma_y}{\sqrt{P}}|U|^{-1}\right)=\frac{G_E}{P}}$$

If P is sufficiently large then (considering the law of large numbers and the distribution properties the measurement noise) the term $\hat{G}_E^{[m]}$ converges to zero, so that is eliminated, i.e.:

$$E\{\hat{G}^{[m]}\} = E\left\{\hat{G}_{BLA}^{[m]} + \hat{G}_S^{[m]} + \mathcal{N}\left(0, \frac{\sigma_y}{\sqrt{P}}|U|^{-1}\right)\right\} = G_{BLA} + G_S^{[m]} \tag{30}$$

The partial FRM estimate is given by:

$$\hat{G}^{[m]} = \frac{1}{P}\sum_{p=1}^{P} \hat{G}^{[m][p]} = \frac{1}{P}\sum_{p=1}^{P} Y_{measured}^{[m][p]} U^{[m]^{-1}} \tag{31}$$

The improved covariance of the partial FRM estimate is given by:

$$\hat{\sigma}^2_{\hat{G}^{[m]}} = \frac{1}{P}\sum_{p=1}^{P} \frac{|\hat{G}^{[m][p]} - \hat{G}^{[m]}|}{P-1} \tag{32}$$

The additional normalization with P is needed when an improved covariance (noise) estimate needs to be shown for the experiment containing P periods (blocks). This term corresponds to G_E/P. If the user wants to see the covariance (noise) with respect to one period (block) one has to multiply with P. In other words, averaging over repeated blocks results in an improvement of the SNR.

Because the stochastic nonlinear contribution $\hat{G}_S^{[m]}$ does not vary over the P repetition of the same realization we have to average over the M different realizations, such that:

$$\hat{G} = \frac{1}{M}\sum_{m=1}^{M} \overbrace{\hat{G}^{[m][p]}}^{measured\ FRF} = \frac{1}{M}\sum_{m=1}^{M} (\overbrace{\hat{G}_{BLA}}^{\substack{FRF \\ fixed}} + \overbrace{\hat{G}_S^{[m]}}^{\substack{nonlinearity \\ varies\ over\ m}} + \overbrace{\hat{G}_E^{[m]}}^{\substack{noise \\ varies\ over\ m}}) = \hat{G}_{BLA} + \frac{1}{M}\sum_{i=1}^{M} (\underbrace{Y_S^{[m]}}_{\mathcal{N}(0,\sigma_S)} + \underbrace{E^{[m]}}_{\mathcal{N}\left(0,\frac{\sigma_y}{\sqrt{P}}\right)})|U|^{-1} =$$

$$\hat{G}_{BLA} + \underbrace{\hat{G}_s/M}_{\mathcal{N}\left(0,\frac{\sigma_S}{\sqrt{M}}|U|^{-1}\right)} + \underbrace{\hat{G}_E/MP}_{\mathcal{N}\left(0,\frac{\sigma_y}{\sqrt{MP}}|U|^{-1}\right)} \tag{33}$$

If M is sufficiently large, then the nonlinear noise source converges to zero, so that term is eliminated. After the multidimensional averaging the BLA estimate is obtained, i.e.:

$$E\{\hat{G}\} = E\left\{\hat{G}_{BLA} + \left(\mathcal{N}\left(0, \frac{\sigma_S}{\sqrt{M}}\right) + \mathcal{N}\left(0, \frac{\sigma_y}{\sqrt{MP}}\right)\right)|U|^{-1}\right\} = G_{BLA} \tag{34}$$

The BLA estimation is obtained as follows:

$$\hat{G}_{BLA} = \frac{1}{M}\sum_{m=1}^{M} \hat{G}^{[m]} = \frac{1}{M}\sum_{m=1}^{M} \frac{1}{P}\sum_{p=1}^{P} \hat{G}^{[m][p]} = \frac{1}{M}\sum_{m=1}^{M} \frac{1}{P}\sum_{p=1}^{P} Y_{measured}^{[m][p]} U^{[m]^{-1}} \tag{35}$$

The improved covariance estimate is given by:

$$\hat{\sigma}^2_{\hat{G}_{BLA}} = \frac{1}{M}\sum_{m=1}^{M} \frac{|\hat{G}^{[m]} - \hat{G}_{BLA}|^2}{M-1} \tag{36}$$

The improved estimate of the noise covariance is given by:

$$\hat{\sigma}^2_{\hat{G}} = \frac{1}{M}\sum_{\mathrm{m}=1}^{M} \frac{\sigma^2_{\hat{G}^{[m]}}}{M} \tag{37}$$

The estimate of the noise covariance $\hat{\sigma}^2_{\hat{G}}$ is calculated from the averaged sample variance of each FRM realization. The total variance of the FRM $\hat{\sigma}^2_{\hat{G}_{BLA}}$ is calculated from the sample variance of each different partial BLA estimates $\hat{G}^{[m]}$.

At this point it is important to stretch the fact that the above-mentioned noise sample calculations of the BLA are only valid when the input signals are measured with an SNR larger than or equal to 20 dB, see Section 2.1. In [38] it has been shown that the systematic errors introduced by the input noise both on the estimated FRF and its confidence bounds are negligibly small.

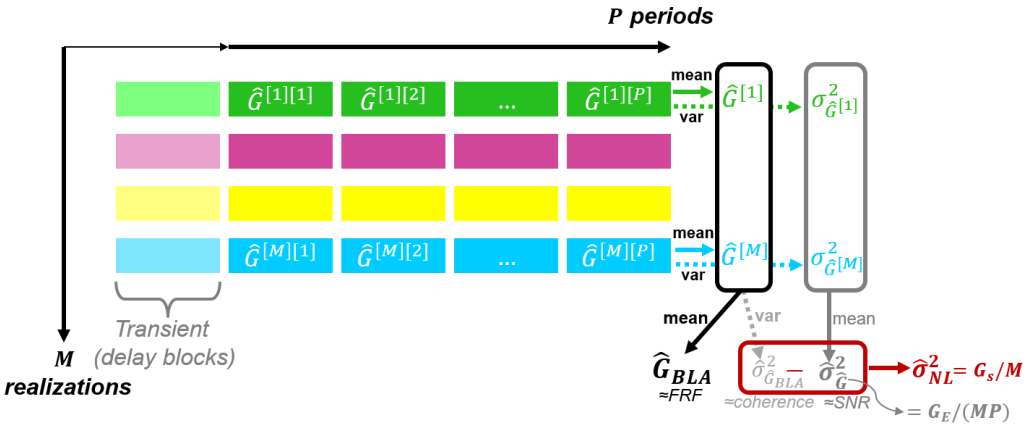

Fig 13. Evaluation of BLA estimate with the help of multidimensional averaging.

6.4. *Normalization modes*

The difference between the total variance and the noise variance is an estimate of the variance of the stochastic nonlinear contributions $\hat{\sigma}^2_{NL} \approx \left(\hat{\sigma}^2_{\hat{G}_{BLA}} - \hat{\sigma}^2_{\hat{G}}\right)$. When the user intends to see how much nonlinearty is present on an arbitrary experiment, one has to consider M-times $\hat{\sigma}^2_{NL}$ such that $\hat{\sigma}^2_{\hat{G}_S} \approx M\hat{\sigma}^2_{NL}$. The same applies to the noise information. $\hat{\sigma}^2_{\hat{G}_E}$ provides an improved estimate of the noise on the FRM. When the user intends to see how much noise is present on an arbitrary experiment, one has to consider MP-times $\hat{\sigma}^2_{\hat{G}}$ such that $\hat{\sigma}^2_{\hat{G}_E} \approx MP\hat{\sigma}^2_{\hat{G}}$.

Thus, for one arbitrary chosen period (block), the expected level of nonlinearities is given:

$$\sigma^2_{\hat{G}_S} = M\left(E\{\sigma^2_{\hat{G}_{BLA}}\} - E\{\hat{\sigma}^2_{\hat{G}}\}\right) \approx M\left(\hat{\sigma}^2_{\hat{G}_{BLA}} - \hat{\sigma}^2_{\hat{G}}\right) = M\hat{\sigma}^2_{NL} \tag{38}$$

and the noise level is given by:

$$\sigma^2_{\hat{G}_E} \approx MP\hat{\sigma}^2_{\hat{G}} \tag{39}$$

For all experiments the impact of nonlinearities on the BLA model is given by:

$$\sigma^2_{NL} = E\{\sigma^2_{\hat{G}_{BLA}}\} - E\{\hat{\sigma}^2_{\hat{G}}\} = \frac{\sigma^2_S}{M} \approx \left(\hat{\sigma}^2_{\hat{G}_{BLA}} - \hat{\sigma}^2_{\hat{G}}\right) \tag{40}$$

and the noise level is given by:

$$\hat{\sigma}^2_{\hat{G}} = \frac{1}{M}\sum_{i=1}^{M} \frac{\sigma^2_{\hat{G}[i]}}{M} \tag{41}$$

Authors recommend checking always the period-wise (block-wise) nonlinearity levels as a first step. Using many realizations and simultaneously showing the improved $\hat{\sigma}^2_{NL}$ nonlinearity level might give a wrong message to the user since its value converges to zero. An illustration of these two normalization modes are shown in Fig 14. The period-wise normalization mode is especially useful when the end-user wants to use a simple linear model for his simulation/control purposes. In this case the error levels would be in order of SNLR (signal to nonlinearity ratio). If the end-user decides to opt for an appropriate nonlinear model the error levels would be in order of SNR. The improvement using an advanced nonlinear model would be approximately the difference between the SNR and SNLR (see Fig 14.). The numerical computation of SNR and SNLR values are provided in Section 7.3.

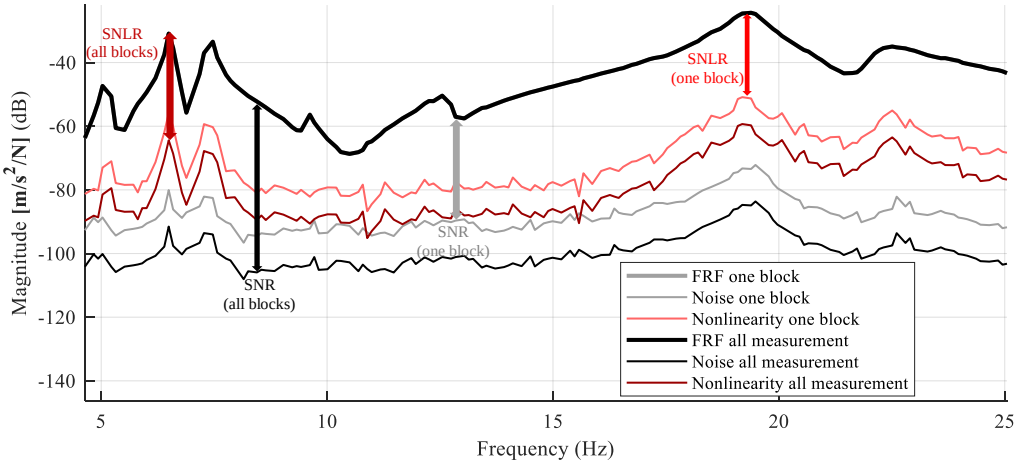

Fig 14. The best linear approximation of a ground vibration testing experiment of an F16 air fighter. The thick black line shows the FRF of the BLA. The red line shows the level of nonlinear distortion and the thin black line shows the noise. The darker shades refer to the normalization mode showed for the overall averaged measurement, the lighter shades refer to the normalization with respect to one period (block).

6.5. Variance estimates versus coherence function estimates

The classical H1 FRF estimation framework suggest calculating the coherence function for each frequency line [24]. When the coherence function gives one it means that there is 100% linear correlation between the measured output and input data. When the coherence is lower than one it indicates the presence of (among others) high level noise and/or transient (leakage) and/or nonlinearities. Because a periodic excitation is used with discarding the delay blocks (transient), it has been made sure that the lack of coherence stands only for the noise and nonlinearities. In the following part the FRM estimation of a battery-operated small aircraft is shown. The measurement is elaborated in Section 8.1

In the classical H1 framework the coherence function (pink thick line in Fig 15.) is used to estimate the FRF measurement's standard deviation (pink thin line). For the numerical computation of coherence function in MIMO case we refer to [39]. Please note that by the use of the proposed BLA framework we can directly estimate the standard deviation and split it to into noise level estimation (black thin line) and nonlinearity level estimation (red thin line) as explained in the multidimensional averaging section of this paper.

With the help of these curves it is possible to tell how much the lack of coherence accounts for the noise and nonlinearity. For instance, the first resonance (around 3 Hz) has an SNR of 35 dB and an SNLR (signal-to-nonlinearity ratio) of 40 dB. This means that at this resonance the main error source is the noise. Looking at the largest resonance (4th resonance at around 12 Hz) one can read that the SNR is around 60 dB and the SNLR is around 30 dB. At this resonance the dominant error source is the nonlinearity.

A further interesting point to highlight is that because periodic excitation is used, it is possible to estimate the standard deviation directly from the data instead. A standard deviation comparison between BLA and H1 is studied in [40]. This comparison indicates that the BLA estimate is more robust – the BLA's standard deviation can reach lower values than the standard deviation of H1.

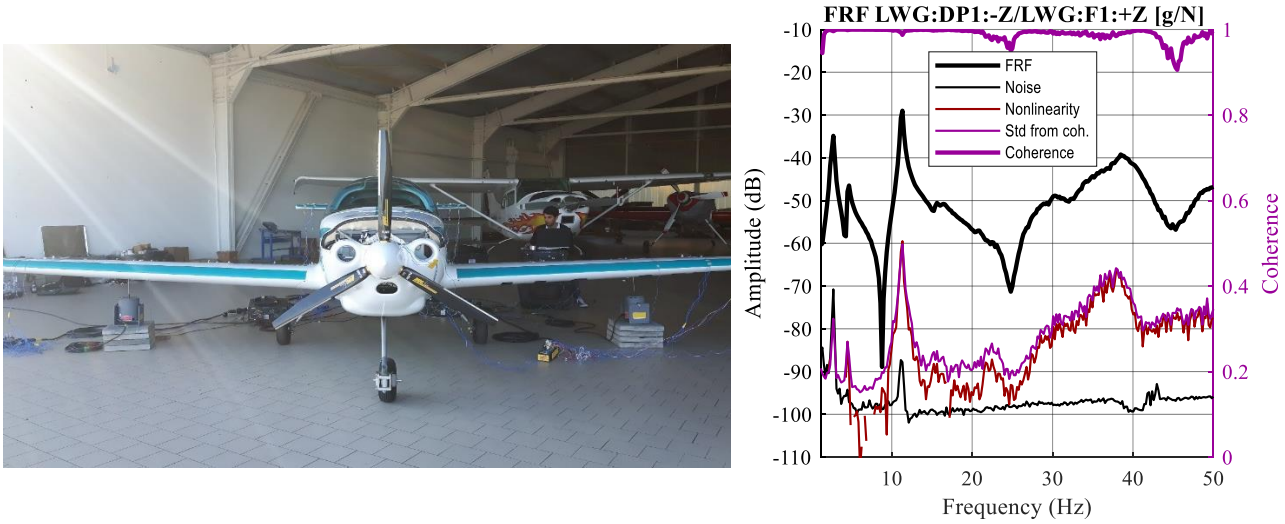

Fig 15. The BLA FRF estimation at high level excitation using the proposed technique – normalized with respect to all periods.

6.6. Coping with transient

6.6.1. Modeling of the transient term

Periodic excitation helps to overcome possible issues with leakage, helps to reduce the noise level, and, when the measurement is sufficiently long, transient contaminated periods can be simple discarded. In some cases, due to the very low damping of the underlying system or insufficient number of periods this discarding technique cannot be used. In '60s windowing methods were developed to suppress the errors to the leakage and transient. However, nowadays the computational power is significantly higher which opened the possibility to use solutions with a better leakage rejection at a cost of making more calculations. If transient is present, one must consider the baseline model (4) instead (3). Combination of (4) and (27) at the excited frequency bins gives

$$Y_{measured}^{[m][p]} = \left(\hat{G}_{BLA} + \hat{G}_S^{[m]} + \hat{G}_E^{[m][p]}\right) U^{[m][p]} + T^{[m][p]} = \left(\hat{G}^{[m][p]}\right)\mathrm{U}^{[m][p]} + T^{[m][p]} \quad (42)$$

where $T^{[m][p]}$ represent the (autonomous) transient term.

Because the FRF and the transient are smooth it is possible to use polynomial approximations such as the Local Polynomial Method (LPM) [20]. The drawback is that the LPM has issues with highly damped systems such that the peaks in the FRFs are usually underestimated. To improve the estimates at a cost of more parameters to be estimated Local Rational Method (LRM) has been suggested [36]. The LRM still uses the property of the smoothness of the FRF and transient transfer function but also uses the fact that they inherently have common poles (which is the difference between LPM and LRM). This paper considers a straightforward, iteration free, direct implementation of LRM. The suggested LRM is also calculated per excited frequency

lines. In the process, a sliding processing window is used with a polynomial degree of d. First, an excited frequency line is selected (frequency index k), this is called the central frequency, this is the middle point of the processing window. Around this frequency line in a $\pm d/2$ radius a narrow band is selected such that this interval is given by

$$r = -round\ down\left(\frac{d}{2}\right) \dots 0 \dots round\ up(\frac{d}{2}) \tag{43}$$

In this band all the (excited and non-excited) frequency lines are used to estimate the transfer functions in polynomial form. The nonexcited lines in this case help to capture the noise behavior. An illustration of the method is shown in Fig 16.

The measured output is given by at the excited frequency index k in a radius of r as follows:

$$\hat{Y}^{[m][p]}_{measured}[k+r] = G^{[m]}U^{[m][p]}[k+r] + T^{[m][p]}[k+r] + E^{[m][p]}[k+r] = \frac{G_p}{D}U^{[m][p]} + \frac{T_p}{D} + E^{[m][p]}[k+r] \tag{44}$$

where G_p, T_p, D are polynomials of order d, k is an excited frequency line (here it is the so-called central frequency), and r is a narrow band.

The polynomials are given by:

$$G_p = \sum_{s=0}^{d} g_s r^s = \underbrace{\overbrace{g_0}^{G}}_{G_T} + g_1 r + g_2 r^2 + \dots + g_d r^d \tag{45}$$

$$T_p = \sum_{s=0}^{d} b_s r^s = \overbrace{t_0}^{T} + t_1 r + t_2 r^2 + \dots + t_d r^d \tag{46}$$

$$D = 1 + \sum_{s=1}^{R} d_s r^s = 1 + d_1 r + d_2 r^2 + \dots + d_d r^d \tag{47}$$

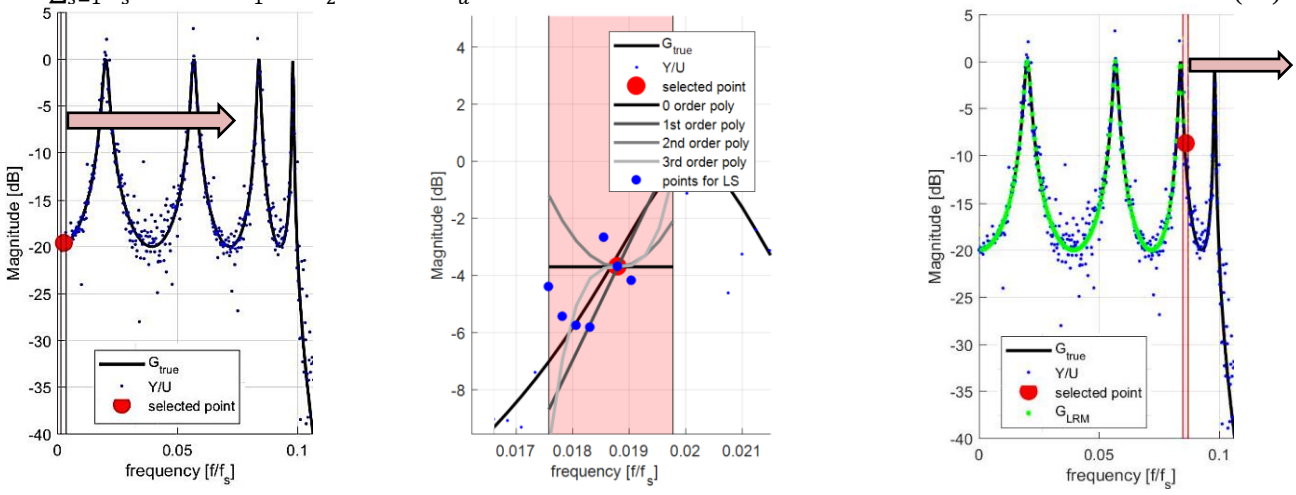

Fig 16. The suggested local rational method. The figure on the left shows the selection of an excited frequency line and the narrow processing band. The middle figure shows the magnification of a such band, together with a conceptual illustration of polynomials. The small blue dots refer to the unprocessed, transient disturbed points of the FRF estimate. On each of these points the LRM method is called. The right figure shows the moving the narrow processing band. The green dots refer to the LRM estimated points.

6.6.2. The cost function

The LRM parameters in (40) are not linear in $\hat{G}^{[m][p]}$ and $T^{[m][p]}$. Multiplying (41) with D makes all parameters linear. The solution is given by:

$$\hat{\theta}_k \triangleq arg\min_{\theta_k} \sum_r \left|Y[k+r]D - G_p U[k+r] - T_p\right|^2 \tag{48}$$

where $\hat{\theta}_k$ is the parameter estimates of the LRM model (i.e. the polynomials) at frequency bin k.

For each frequency line there are $3d+2$ unknown parameters to be estimated ($d+1$ in G_p, $d+1$ in T_p, d in D). This means, for the algorithm to work the frequency in the processing window should be at least $3d+2$ wide (i.e. $|r| \geq 3d+2$). In this work we consider second degree polynomials ($d=2$). The restriction on the width of the processing window also means that in the FRM measurement, in the $-3dB$ bandwidth of the lowest damped mode (the sharpest peak in the FRF) should be at least $3d+2=8$ points measured. At the edges of the FRM measurement (around the first and last excited bins) the processing window should be modified to include at least $3d+2=8$ points.

It is important to stress that the FRF estimates are calculated only at the excited frequency lines, but in the estimation process all the lines are in use.

6.6.3. Illustration

Next, a demonstrative SISO implementation is given for the LS problem (44). The central frequency k is chosen to be 3. The polynomial degree d is 2. The size of the processing window is 8. With elementwise multiplication $\odot$ the following is given:

$$
\overbrace{\begin{bmatrix} Y[0] \\ Y[1] \\ Y[2] \\ Y[3] \\ Y[4] \\ Y[5] \\ Y[6] \\ Y[7] \end{bmatrix}}^{Y} = \overbrace{\underbrace{\begin{bmatrix} 1 & -3 & 9 \\ 1 & -2 & 4 \\ 1 & -1 & 1 \\ 1 & 0 & 0 \\ 1 & 1 & 1 \\ 1 & 2 & 4 \\ 1 & 3 & 9 \\ 1 & 4 & 16 \end{bmatrix}}_{polynomials}}^{place\ in\ matrix\ K} \odot \begin{bmatrix} U[0] & U[0] & U[0] \\ U[1] & U[1] & U[1] \\ U[2] & U[2] & U[2] \\ U[3] & U[3] & U[3] \\ U[4] & U[4] & U[4] \\ U[5] & U[5] & U[5] \\ U[6] & U[6] & U[6] \\ U[7] & U[7] & U[7] \end{bmatrix} \odot \overbrace{\begin{bmatrix} g_0 & g_1 & g_2 \\ g_0 & g_1 & g_2 \\ g_0 & g_1 & g_2 \\ g_0 & g_1 & g_2 \\ g_0 & g_1 & g_2 \\ g_0 & g_1 & g_2 \\ g_0 & g_1 & g_2 \\ g_0 & g_1 & g_2 \end{bmatrix}}^{place\ in\ matrix\ \theta_k} + \overbrace{\underbrace{\begin{bmatrix} 1 & -3 & 9 \\ 1 & -2 & 4 \\ 1 & -1 & 1 \\ 1 & 0 & 0 \\ 1 & 1 & 1 \\ 1 & 2 & 4 \\ 1 & 3 & 9 \\ 1 & 4 & 16 \end{bmatrix}}_{polynomials}}^{place\ in\ K} \odot \overbrace{\begin{bmatrix} t_0 & t_1 & t_2 \\ t_0 & t_1 & t_2 \\ t_0 & t_1 & t_2 \\ t_0 & t_1 & t_2 \\ t_0 & t_1 & t_2 \\ t_0 & t_1 & t_2 \\ t_0 & t_1 & t_2 \\ t_0 & t_1 & t_2 \end{bmatrix}}^{place\ in\ \theta_k}
$$

$$
- \overbrace{\underbrace{\begin{bmatrix} -3 & 9 \\ -2 & 4 \\ -1 & 1 \\ 0 & 0 \\ 1 & 1 \\ 2 & 4 \\ 3 & 9 \\ 4 & 16 \end{bmatrix}}_{polynomials}}^{place\ in\ K} \odot \begin{bmatrix} Y[0] & Y[0] \\ Y[1] & Y[1] \\ Y[2] & Y[2] \\ Y[3] & Y[3] \\ Y[4] & Y[4] \\ Y[5] & Y[5] \\ Y[6] & Y[6] \\ Y[7] & Y[7] \end{bmatrix} \odot \overbrace{\begin{bmatrix} d_1 & d_2 \\ d_1 & d_2 \\ d_1 & d_2 \\ d_1 & d_2 \\ d_1 & d_2 \\ d_1 & d_2 \\ d_1 & d_2 \\ d_1 & d_2 \end{bmatrix}}^{place\ in\ \theta_k} \tag{49}
$$

where $\odot$ refers to the elementwise multiplication. This equation can be rewritten in the well-known LS form as:

$$Y = K\theta_k. \tag{50}$$

This equation can be easily solved with the help of a numerically stable inversion [27].

A measurement example is given in Fig 17. The system under test is the frame of a small vehicle (Siemens Simrod car, see Fig 10) excited from vertical and horizontal directions by shakers. There are in total 50 periods (10 realizations, 5 periods per realization) measured. The illustration shows what happens if only one period of the signal is available.

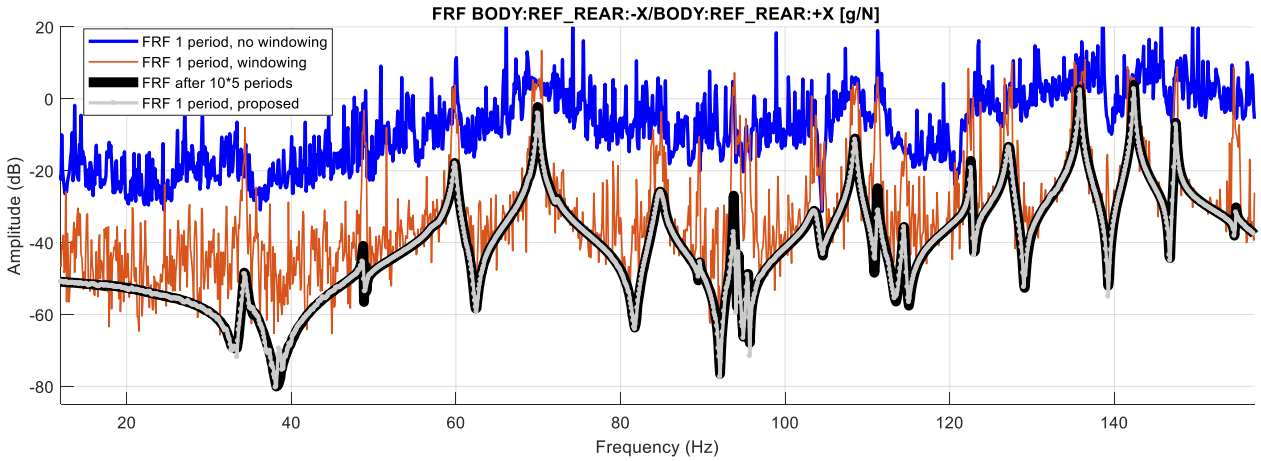

Fig 17. An FRF estimate of a lowly damped vehicle. The black line shows the H1 estimate using fifty periods. The blue line shows the classical H1 estimate using one period, the red line shows the H1 estimate with Hanning windowing using one period. The gray line shows the LRM estimate using one period.

6.7. Actuator characteristics and the advantage of missing harmonics multisine

6.7.1. Nonparametric characterization

In mechanical, control and electrical engineering it is a common (silent) assumption that the actuator (excitation system) is linear. The reference signal generated by a computer or arbitrary function generator is typically fed to the actuator which generates the input signal. A general overview of instrumentation can be seen in Fig 1. A vibration test example of a tire suspension system can be found in Section 4.2 where the reference (voltage) signal is fed to the actuator which is amplifier-shaker combination. The displacement of the hydraulic shaker results in force at the structure being tested. The transfer between the reference (voltage) and input (force) signals is assumed to be linear, and therefore, in general, the (nonlinear) effect of the actuator is not considered, and the reference signal is not measured.

There are two related issues. First, the system under test can have a (mechanical-indirect) feedback connection, for instance, when the actuator shakes the system, the system shakes back. In this case there is a risk for a low-quality measurement due to systematic errors [20], and the model obtained might include the actuator characteristics as well. Second, our experience shows

that the silent assumption on the linearity of the actuator is not always satisfied. Therefore, it is crucial to analyze the actuator as well. For the tree input, two output system illustration given in Section 4.4, the actuator extended version is given in Fig 18.

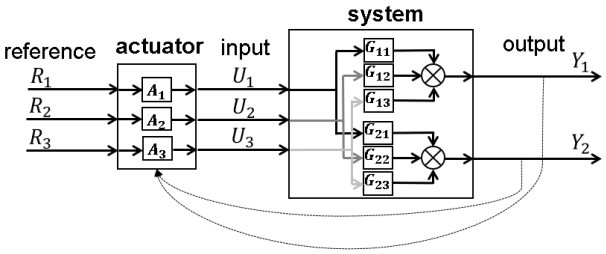

Fig 18. Illustration of an actuator and system with three inputs and two outputs. The dashed lines indicate a possible feedback.

6.7.2. The actuator characteristics

From system identification point of view, the actuator and its transfer functions can be seen as series of SISO systems (see A_1, A_2, A_3 in Fig 18.). For each of these transfer functions the BLA estimate can be calculated (using the corresponding reference-input signals), and the user can be warned if the linearity assumption of the actuator is not satisfied, see Section 2.1. The reference, input signals and the BLA estimate of the hydraulic shaker used in Fig 5. (Section 4.2.) are shown in Fig 19. Observe that the reference signal is flat, the even and odd nonexcited lines fall bellow the noise estimate. The input signal has a non-flat characteristic with increased odd end even nonlinear distortions. The FRF, noise and nonlinear estimates of the BLA clearly show the nonlinear nature of the excitation system.

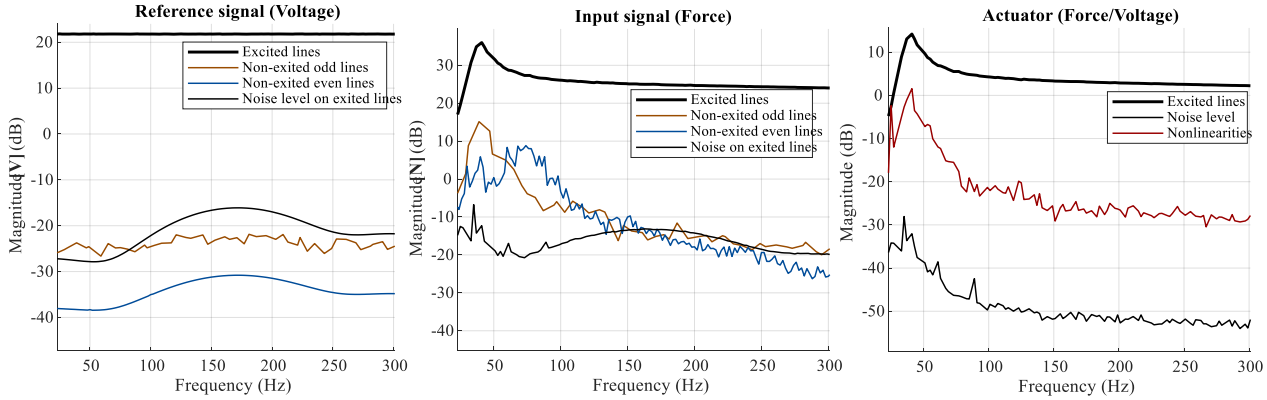

Fig 19. An actuator (hydraulic shaker) characteristic is shown with respect to one period (block). On the left the measured reference signal is shown. In the middle the measured input signal is shown. On the right the BLA estimate of the actuator is shown. Observe that the reference signal is almost linear (around 50 dB SNR, and the nonlinearities are hidden in the noise), where the excitation signal contains already significant amount of nonlinearities.

6.7.3. Reducing the (indirect) feedback effect

If there is a slight (indirect) feedback from the responses to the actuator (see Fig 18.), using cross-power estimates can improve the BLA estimate of the underlying system. In this case without changing the multidimensional averaging process, $\hat{G}^{[m][p]}$ is calculated with the help of (unwindowed) power spectrum estimates [27] as follows:

$$\hat{G}^{[m][p]} = \hat{S}^{[m][p]}_{Y_{measured}R}\left(\hat{S}^{[m][p]}_{UR}\right)^{-1} \tag{51}$$

It is easy to see that by using the deterministic properties of the reference signal one can obtain back (27):

$$E\{\hat{G}^{[m][p]}\} = E\left\{\hat{S}^{[m][p]}_{Y_{measured}R}\left(\hat{S}^{[m][p]}_{UR}\right)^{-1}\right\} = E\left\{\hat{Y}^{[m][p]}_{measured}\mathrm{R}^{[m]}\mathrm{R}^{[m]^{-1}}\mathrm{U}^{[m]^{-1}}\right\} = E\left\{\hat{Y}^{[m][p]}_{measured}\right\}\mathrm{R}^{[m]}\mathrm{R}^{[m]^{-1}}E\left\{\mathrm{U}^{[m]^{-1}}\right\} = \hat{Y}^{[m][p]}_{measured}\mathrm{U}^{[m]^{-1}} \tag{52}$$

This method is closely related to the instrumental variables problem formulation [41].

6.7.4. Improving output measurements

The basic idea of using odd random-phase multisines is to detect even and odd nonlinear contributions, in-band and out-band nonlinearities. However, the interpretation of the levels on the detection lines at the output can be jeopardized, if the actuator is imperfect, see, for example, Fig 19. If there is power on the detection lines at the input signal power, then the output signals will contain not only the nonlinearities due the system but also the nonlinear contributions of the actuator. The proposed framework is suitable to clean-up the output spectrum with the impurities of the actuator, as illustrated in Fig 20. First, the linear output spectrum is estimated on the detection lines with the help of the interpolated BLA estimation and input signal as follows:

$$\hat{Y}^{[m][p]}_{simulated} = \mathrm{G}_{\mathrm{BLA}}\mathrm{U}^{[m][p]} \tag{53}$$

Then, the measured output is corrected at the non-excited lines as follows:

$$\hat{Y}^{[m][p]}_{measured-corrected} = \hat{Y}^{[m][p]}_{measured} - \hat{Y}^{[m][p]}_{simulated} \tag{54}$$

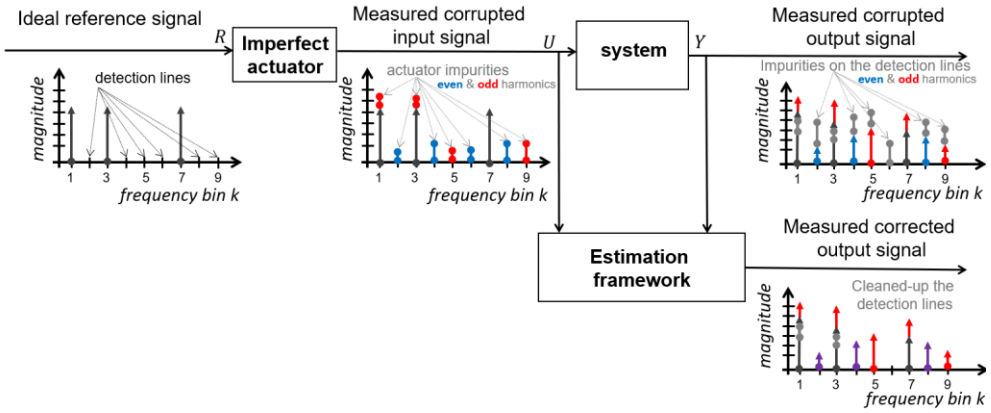

Fig 20. Illustration of the output harmonics correction method in the presence of an imperfect (nonlinear) actuator.

The cleaned-up output spectrum then can be used to analyze the nonlinearities [20]. In this work it has been verified that the extended MIMO methodology works well on MIMO simulations and measurements. An illustration is shown in Fig 21. Observe that the raw output measurements contain significant amount of nonlinear distortions, based solely on this observation, a wrong conclusion can be easily drawn: all FRFs of the observed system are nonlinear. With the help of the proposed process, the effect of the imperfect actuator can be cleaned up resulting in linear output channel one reveling the true nonlinear nature of the underlying system.

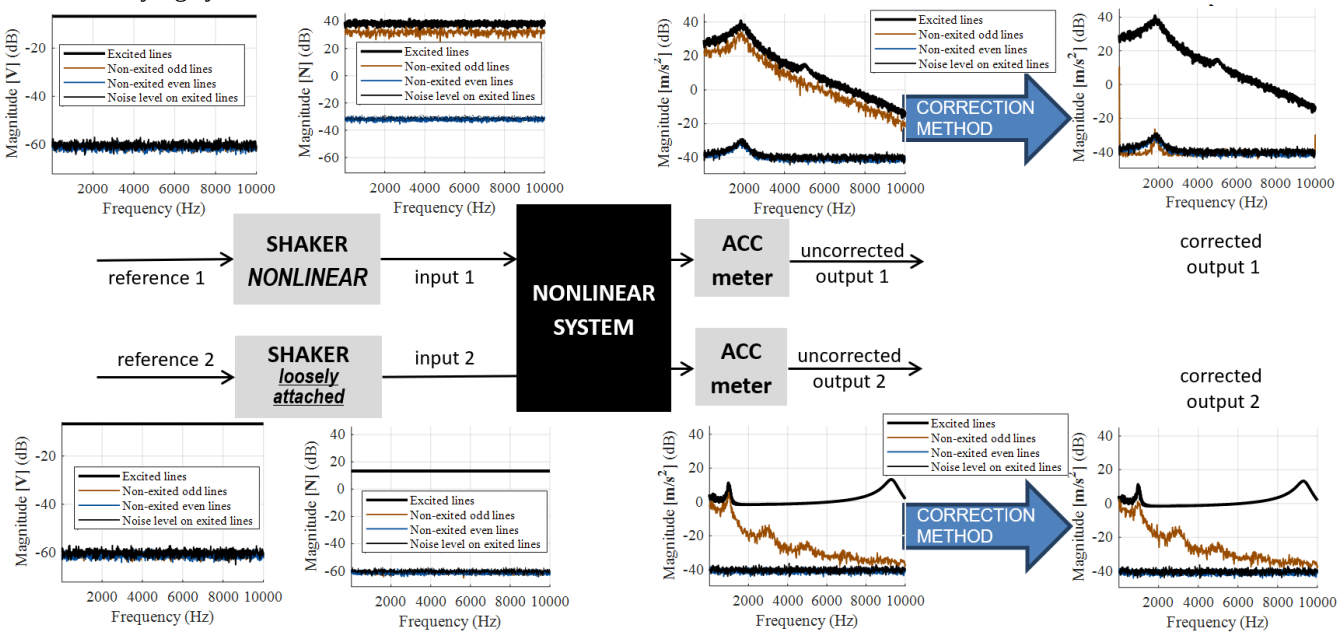

Fig 21. Illustration of the proposed output spectrum correction method. The reference signals are fed to a 1) nonlinear shaker (with cubic spring behavior) and to a 2) loosely attached shaker. The first input signal contains significant odd nonlinear distortions, the second input signal has higher noise level. Observe that both uncorrected outputs contain significant odd nonlinearities but after the correction method applied only the second output channel contains nonlinear distortions.

7. Post-processing

7.1. Introduction

In the previous section, the BLA FRM, its nonlinearity and noise estimates have been obtained but not yet analyzed. According to the traditional post-processing approach, an expert user has to take a look at each of the FRM elements and has to manually analyze the transfer function, noise and nonlinearity estimates. This process, on one hand, requires experienced user and significant amount of time which grows with the number of input and output channels, on the other hand, the project schedules are tight, and most of the time expert users are not available.

The time and effort invested in the analysis, however, can be dramatically reduced by (semi-)automatically post-processing the results obtained from the previous sections. Depending upon the target application, it is also possible to analyze the data only

in the frequency domain of interest, for instance, around the most important poles (modes). Because different applications can have different quality needs, it is recommended to use predefined application-oriented profiles. Using the proposed methodology, it is possible to have the same automated framework for large variety of applications.

7.2. Significance metrics

As stressed earlier, the key of the proposed framework is the (semi-)automatic processing of all available information. The user of the nonparametric estimation framework is expected to get (customized) warnings only if a significant event occurs. The significance is defined in the application profile, calculated in the frequency domain and can be defined as follows.
The warning of significance should appear, when the nonlinearity (in the selected frequency band of interest) lies

- above the noise level estimate, or
- in the proximity of the signal (FRF) level estimate

with

- a predefined absolute value, (e.g. 40 dB), or
- a certain amount times the standard deviation of the noise, or
- a positive outcome of a statistical hypothesis test

when

- there is at least one frequency line (narrow frequency band), or
- a certain percentage of the area is reached.

This significance analysis can be done for the system and actuator FRFs, the input, (corrected) output and reference signals.

7.3. Input, reference and output signals

- *The SNR of the (input) signal measurement*

It is advised to check the excitation signal measurement quality as well. As mentioned earlier, the period-wise SNR should be at least 20 dB in order to be able to neglect the systematic errors of the FRM estimate introduced by the input noise.
A robust noise estimate of the input signal can be obtained by using the multidimensional averaging methodology presented in Section 6.3. First, averaging over P periods (blocks) in realization l the noise estimate is given by:

$$\hat{\sigma}^2_{U^{[l]}} = \frac{1}{P}\sum_{p=1}^{P} \frac{\left|U^{[l][p]} - \hat{U}^{[l]}\right|^2}{P-1} \tag{55}$$

where l accounts for all realization M and phase rotation n_i,and $\hat{U}^{[l]}$ is the mean value.
Next, averaging over M times n_i realizations gives the improved noise estimate with respect to the whole measurement:

$$\hat{\sigma}^2_{U} = \frac{1}{Mn_i}\sum_{i=1}^{Mn_i} \frac{\hat{\sigma}^2_{U^{[l]}}}{Mn_i} \tag{56}$$

For one arbitrary chosen period (block), the expected noise level is given by:

$$\sigma^2_{U_P} \approx Mn_i P \hat{\sigma}^2_U \tag{57}$$

The above-mentioned calculation can be used for estimating the noise levels on the output and reference signals as well.
The SNR estimate (per frequency line) can be calculated with the help of the absolute averaged input signal $|\hat{\mathrm{U}}|$ as:

$$\widehat{SNR}_U \approx \frac{|\hat{\mathrm{U}}|}{\sqrt[2]{\sigma^2_{U_P}}} \tag{58}$$

where $\left|\hat{\mathrm{U}}\right| = \frac{1}{Mn_i}\sum_{i=1}^{Mn_i} |\hat{U}^{[l]}|$.
Of course, when the application requires, the expected SNR level(s) can be set higher.

- *Dependency of the input signal measurement*

As explained earlier, the FRM estimation requires uncorrelated excitation signals. At the pre-processing step, there is already a dependency check-up proposed, see Section 5.2. Because the user can decide to continue the processing, it is important to stress that the results are obtained using correlated signals.

- *Different units and noise characteristics*

In most of the applications, the input units are the same. For instance, when a vehicle is tested using shakers, at each input channel the force signals are measured. It is the same situation with the output signals. For the FRM estimation user has to (manually) indicate which measurement channels correspond to the reference, input and output signals. Different quantities in these signals usually indicate mix-up in the choice of the signals.
Further, same sensor types have similar noise characteristics. If a measurement channel has significantly higher noise level, it usually indicates imperfect attachment of the sensor, sensory fault or issues with cable connections. To this end, significance metrics defined in Section 7.2 can be easily amended for including noise characteristic check-up.

- *Even and odd nonlinearities*

Using odd random multisines it is easy to detect even and odd nonlinear contributions, in-band and out-band nonlinearities as explained in Section 4.3 and 6.7.4. The significance check-up in Section 7.2 should include the analysis of even and odd nonlinear contributions of the (corrected) output measurement, and SNLR (Signal to Nonlinearity Ratio) and NNLR (Noise to Nonlinearity Ratio) can be defined for both even and odd nonlinearities by substituting the corresponding values in (51)-(54).

7.4. BLA FRM and actuator FRFs

- *SNR*

It is crucial that an SNR of the FRM is estimated. When SNR value in a given region is too low, then the FRF estimate in that region is not a reliable, and therefore the nonlinearity estimate will be not reliable as well.

- *Nonlinearities*

It is one of the important tasks of the post-processing step is to warn the user if significant level of nonlinearities is present. The significance is calculated using significance metrics defined in Section 7.2,. SNLR (Signal to Nonlinearity Ratio) and NNLR (Noise to Nonlinearity Ratio) can be calculated as well. The interpretation of such quantities is detailed in Section 6.4 and 6.5.

8. Measurement example

8.1. Aircraft testing

This section provides an experimental illustration on the ground vibration testing (GVT) measurement of a battery-operated small aircraft. The measurement setup (see Fig 22.) consists of 2 shakers–2 force cells and 91 acceleration sensors. The sampling frequency is 200 Hz. The period length is 1024 resulting in a frequency resolution of 0.1953 Hz. The smallest excited frequency is 1.1719 Hz, the highest excited frequency is 50.7813 Hz.

There are eight different multisine realizations for each input channel per experiment. Each multisine realization is repeated 3 times. As explained earlier, the extra experimental blocks (necessary to solve the MIMO equations) are obtained by orthogonal phase shifts. Thus, there are in total $M \cdot P \cdot n_i = 8 \cdot 3 \cdot 2 = 48$ blocks.

To analyze the measurements, the post-processing methodology described in Section 7. is used. In this case, the nonlinearity significance trigger is set as 1) the nonlinearty estimate is in $20\ dB$ proximity of the FRF estimate OR 2) the nonlinearity is $20\ dB$ higher than the noise, for at least 10 frequency lines (narrow frequency band).

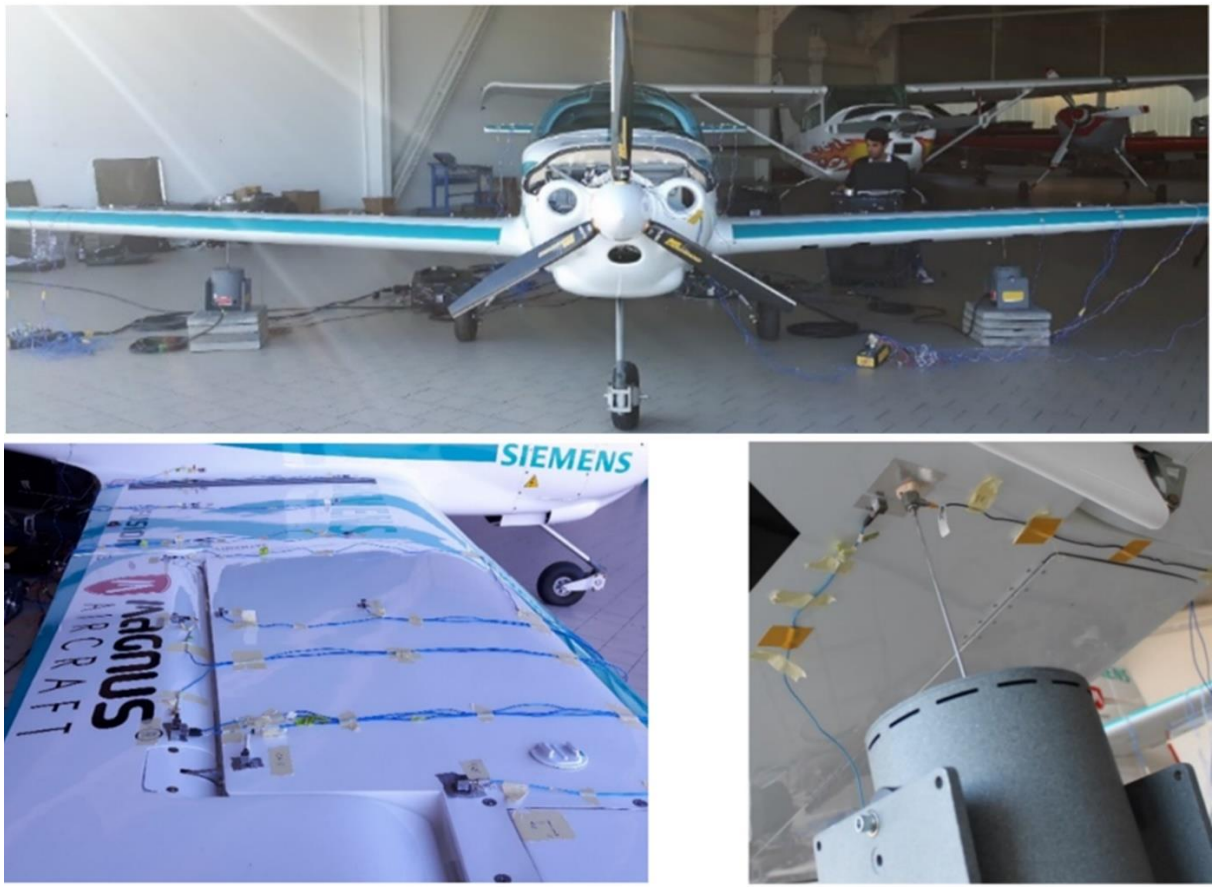

Fig 22. The measurement setup and instrumentation of the GVT of eFusion aircraft.

In order to ensure that the measured signals are in the steady-state, a simple transient check-up is performed (similarly to Fig 10.), and it turned out that only the first block is disturbed by the transient, so each first block (period) in every realization/phase rotation is discarded.

The GVT measurement has been executed at three different levels. Fig 23. shows the excitation signals with the highest level in the frequency domain with respect to one period. The excitation force is measured with approximately 65 dB SNR. This

SNR is sufficiently good to fulfil the assumption on the precise excitation signal measurement. Further, in order to simplify the analysis, the output channels and FRFs are shown at the driving points only. The output (acceleration) measurement is shown in Fig 24. Observe that at the excitation signal no nonlinearities have been detected, but the output signals contain significant nonlinearities with odd nonlinearity dominance.

Fig 25. shows the driving point (symmetrical components of the FRM) and reciprocal FRFs at low and high level of excitation. It can be clearly observed that FRFs differ a lot from each other. This clearly indicated the presence of nonlinearities.

Observe in the following figures that significant nonlinearities are detected, and there is an SNR problem with the output signal measurement in low frequencies resulting in an SNR warning at the FRM estimates as well. The noise and nonlinearity estimates are shown with respect to one period. In this case, if the end-user decides to use a simple linear model in his application, the error levels will be in the order of SNLR (see Fig 25.). If the end-user decides to opt for an appropriate nonlinear model, the error levels could be dropped to SNR level. The improvement using an advanced nonlinear model is approximately the difference between the SNR and SNLR levels (see Fig 25.).

It is interesting to mention is that the anti-diagonal FRFs have a significantly higher nonlinearity level (lower SNLR levels) than in the diagonal FRFs. Frequency-wise the first FRF has the largest area covered with significant nonlinearities. The last FRF behaves almost linearly at low level of excitation.

A discussion related to the coherence function illustrated on this measurement can be found in Section 6.5. Different normalization modes are discussed in Section 6.4.

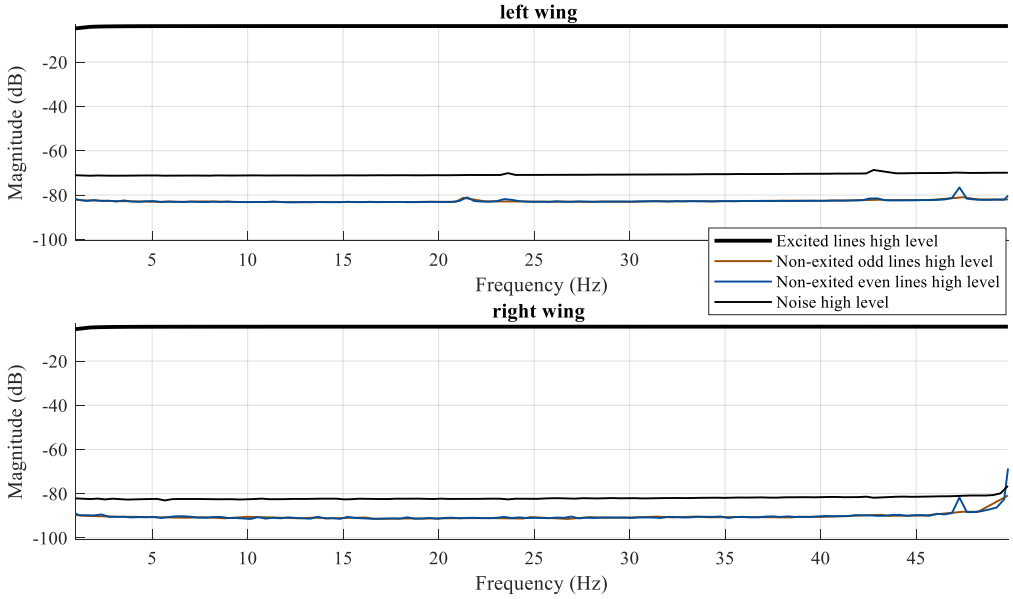

Fig 23. The input (force) signal measured in frequency domain at high amplitude level.

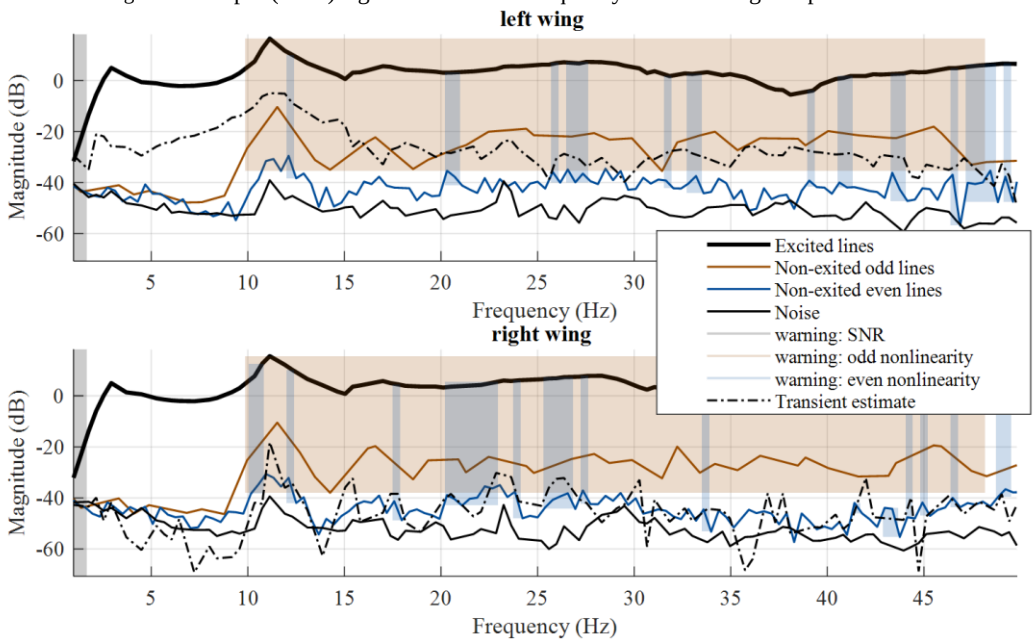

Fig 24. The output (accelaration) signal measured in at high amplitude level, including automatic warnings and transient estimates.

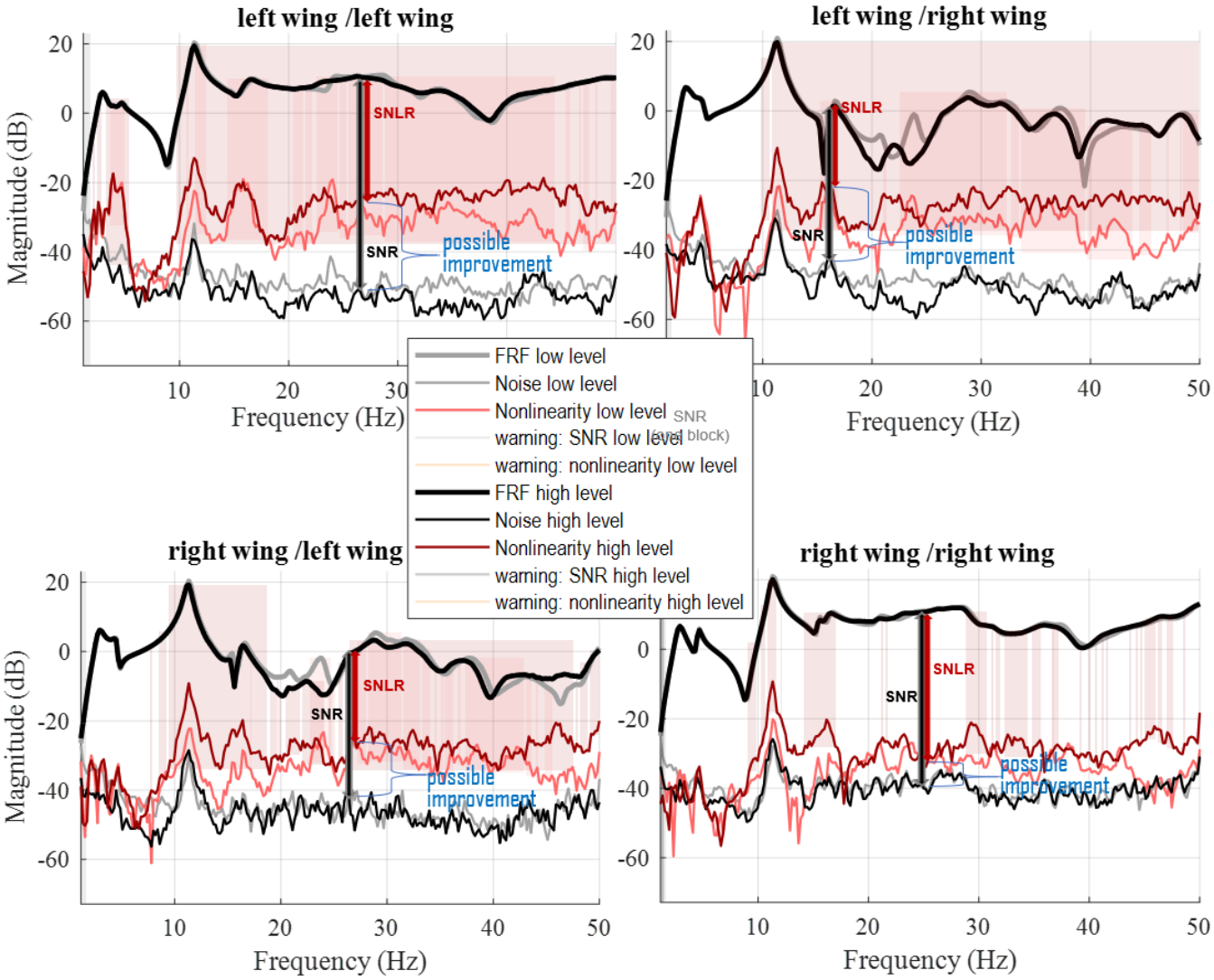

Fig 25. FRFs estimated at the low and high excitation levels.

8.2. Application to satellite testing

This section concerns a direct field acoustic excitation (DFAX) experiment. DFAX is a method to perform environmental acoustic tests [42]. It consists in reproducing the sound field inside a spacecraft vehicle's fairing using an array of electrodynamic loudspeakers. In order to ensure the accurate reproduction of the spatial correlation characterizing such pressure field, during the test, the actuators need to be actively controlled. Therefore, microphones are used to provide pressure error signals, namely, the comparison between the measured pressure responses and the multiple test references. The measurement setup is shown in Fig 26. One of the most sensitive aspects of the DFAX control strategy is the system identification: a low-level test conducted before the qualification. This is because the strategy used for the system identification determines the resultant uncertainties of the experimental and non-parametric model of the electro-acoustic system used to excite the structure. Such model is then used to design the electrical signals driving the array of loudspeakers (i.e. drives) to reach the qualification sound pressure level. A poor model of the electro-acoustic system turns into poor drives and, consequently, into large sound pressure error signals.

In the measurement two multisine experiments for the six drives (excitation channels) have been executed at (relatively) low and a little bit higher power level. The analysis was conducted on both excitation levels. A launch test validation is done using the FRM estimate obtained at higher level of excitation, cross-validated on an experiment where the output level was about 40 dB above the excitation level used for estimation (to reach the qualification level). In the experiment there were 3 periods, 7 realizations and 6 phase rotations applied, the sampling frequency was 51.2 kHz, number of samples in a block is 16384. Unfortunately, after the measurement campaign it turned out that the measurement is contaminated by enormous transient due to fade-in, fade-out process (in this application, fade-in/fade-out cannot be avoided due to safety requirements) such that the first and last realizations are quasi lost, and in the intermediate realizations the transient is 1,5 blocks (periods) long, therefore the transient elimination process has been used [43].

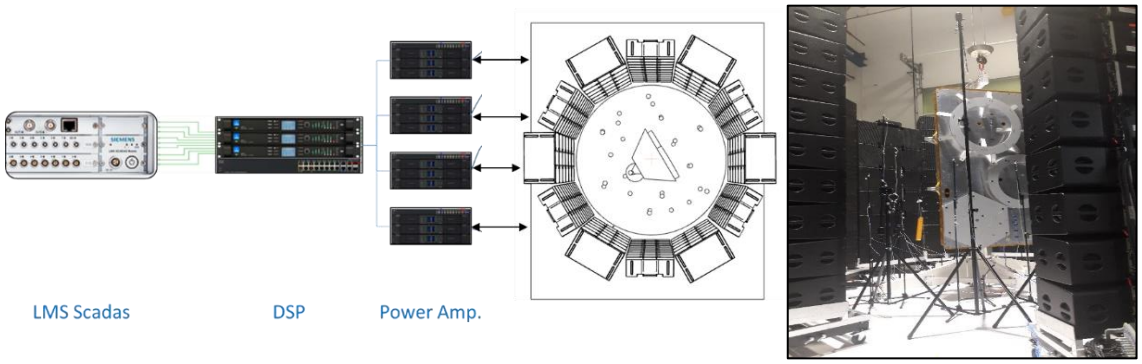

Fig 26. Simcenter SCADAS and electroacoustic system for DFAX.

The magnitude spectra of the measured excitation signals are shown in Fig 27. (left side) at low and higher levels with an approximate overall signal level difference of 6 dB. The reference signals have customized magnitude characteristics. Gray dots show the corresponding noise level estimates, which allows us to give rough estimate of the SNR (around 70 dB). Orange and blue dots refer to the odd and even nonlinearities on the non-excited detection lines (the frequency bins where the type of nonlinearities can be captured). Despite the good SNR, there are some even nonlinearities presented in a magnitude of 25 dB w.r.t. noise level. Apart from this, the nonlinearities have limited effect – since they are at the order of noise level.

The output spectra – microphone outputs – are shown in the right side of Fig 27. The output measurement has significantly lower SNR: around – 45 dB at low, and around -30 dB at high frequencies.

The microphone is governed by even nonlinearities, which ones become especially dominant at mid and higher frequencies and their levels are even more dominant at the higher excitation profile. This indicates that there will be no significant changes in the dynamics when the underlying structure is operated at various power levels, and this would also allow to design a simplified (linear) controller because even nonlinearities can be seen as a special (process) noise: the FRF estimates look more or less noisier by varying the excitation level but the main dynamics remain the same. Changing resonances are usually do the odd nonlinearities. In order to verify the microphone measurements, several accelerometers have been placed on the structure. By processing the measurements same conclusions have been reached.

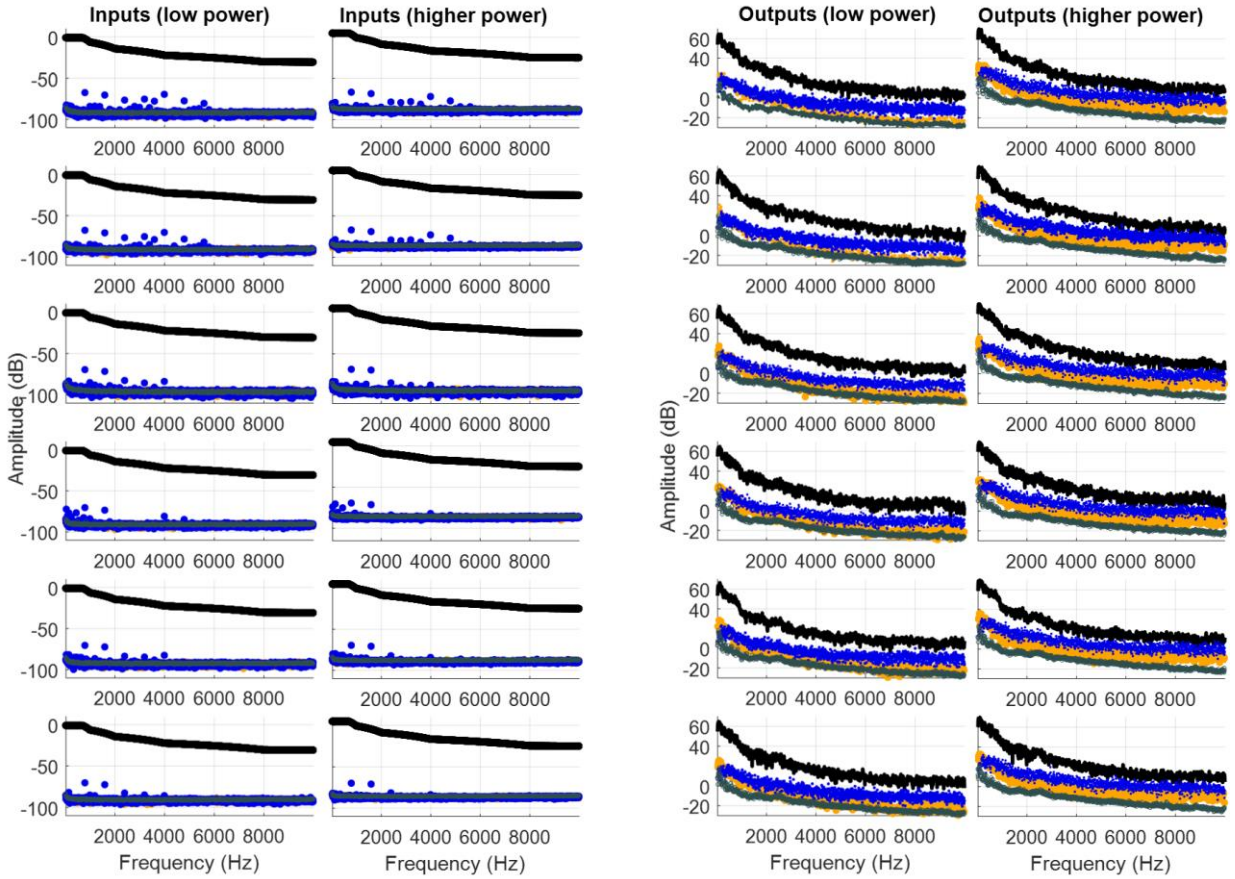

Fig 27. Magnitude of electrical inputs and acoustic outputs are shown. The measured excitation spectra are shown for low level and higher levels (black lines) together with the estimated noise levels (gray dots), even (blue dots) and odd (orange dots) nonlinearities.

Since the controlled input and output channels have similar characteristics, the analysis can be focused on a single FRF. The FRF is measured with high noise level due to unexpected transients and nonlinearities, however, the noise level and the nonlinearities can be clearly distinguished (with a relative difference of 15 dB).

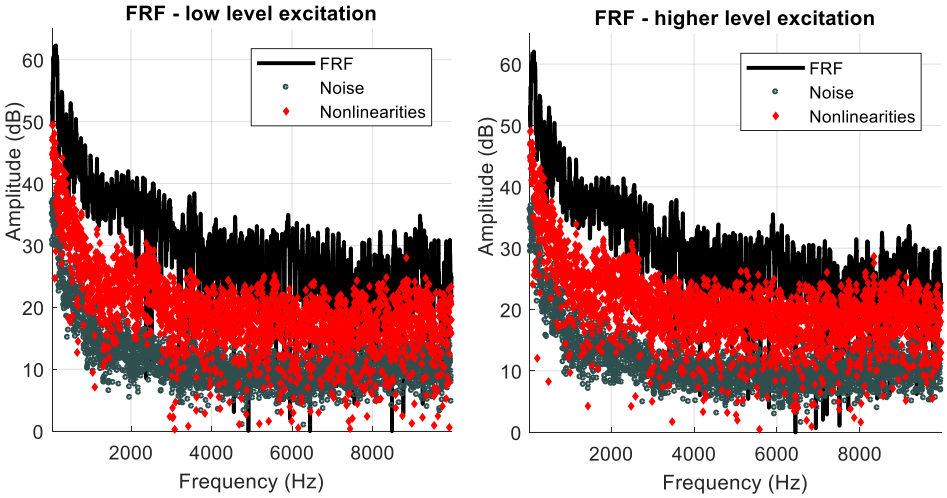

Fig 28. Electroacoustic FRF [Pa/V]. The measured excitation spectra are shown for low level (on the left side) and high levels (on the right side) together with the estimated noise (grey dots), and nonlinearty (red diamonds) levels.

Despite the high level of nonlinearities and the enormous transient level, the BLA approach resulted in an acceptable linear model. Next, it is cross validated on an independent dataset and is compared to the traditional H1 estimate using periodic random noise excitation (classical multisines). In the cross validation the estimated outputs are compared to the measured output where the BLA estimate results in around 6 times smaller relative rms error. Fig 29 shows the cross-validation results magnified around the lower frequencies which are more significant is terms of the application.

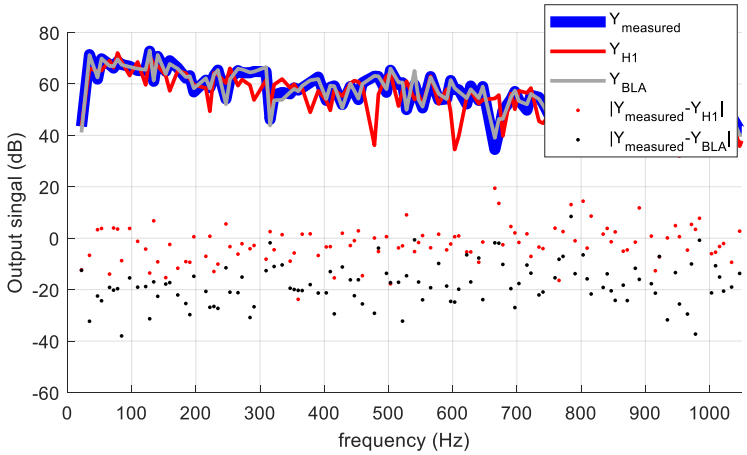

Fig 29. Comparison between estimated and measured magnitudes of acoustic output signals at the frequency band of interest.

9. Conclusions

In this work a MIMO Best Linear Approximation framework was developed to provide a user-friendly automated interpretation of the nonlinear behavior of MIMO measurement data by extracting user relevant information. The proposed framework (and its toolbox implementation) has been tested on various simulations and real-life measurements, and it turned to be useful for measuring and modeling FRFs because:

- it requires minimal user-interaction:
  - the excitation signal parameters are set automatically,
  - the segmentation and processing of the measured data are automated,
  - the results are semi-automatically analyzed, and
  - expert user is not needed.
- orthogonal excitation signals have been provided
  - to optimally excite structures with multiple inputs,
  - to improve the SNR,
  - to better characterize the underlying system,

    - to avoid spectral leakage, and
    - to overcome the issues with transient.
- the reference, input and output measurements were nonparametrically characterized
    - to provide noise models,
    - to provide nonlinear models, and
    - to provide transient models.
- the actuator system is characterized
    - to better characterize the underlying system, and
    - to improve the output measurement quality in case of nonlinear actuator and/or feedback.
- advanced frequency response matrix estimation
    - is simple but robust estimation process,
    - the coherence function virtually slit up into noise and nonlinearity level information, and
    - at each excitation level noise and nonlinearity information can be retrieved.
- user-defined variables profiles can be used
    - to adapt towards the specific needs of the application area,
    - to automatically indicate presence of significant nonlinearities and
    - to automatically indicate presence of measurement quality issues.
- automated fault detection process warns the user when
    - the reference/input signals are correlated,
    - automated data segmentation is not possible,
    - there is a mismatch between the measurement and metainformation, and
    - sensory fault is detected.

Using the provided information an inexperienced user can easily

- decide, if the underlying system is linear or not,
- decide if the linear framework is still accurate (safe) enough to be used, and
- predict how much can be gained using an advanced nonlinear model instead of using the linear framework.

10. Acknowledgements

This work was funded by the VLAIO Innovation Mandate project number HBC.2016.0235.

11. References

[1] G. Kerschen, K. Worden, A.F. Vakakis, J.-C. Golinval, "Past, present and future of nonlinear system identification in structural dynamics,," *Mechanical Systems and Signal Processing*, vol. 20, no. 3, pp. 505-592, 2006.

[2] K. Worden, G.R. Tomlinson, Nonlinearity in Structural Dynamics: Detection, Identification and Modelling,, Bristol : Institute of Physics Publishing, 2001.

[3] J. Schoukens, K. Godfrey, M. Schoukens, "Nonparametric data-driven modeling of linear systems: estimating the frequency response and impulse response function," *IEEE Control Systems Magazine*, vol. 38, no. 4, pp. 49-88, 2019.

[4] J. Schoukens, L. Ljung, "Nonlinear System Identification: A User-Oriented Road Map," *IEEE Control Systems Magazine*, vol. 39, no. 6, pp. 28-99, 2019.

[5] P. Fargette, U. Füllekrug, G. Gloth, B. Levadoux, P. Lubrina, H. Schaak, M. Sinapius, "Tasks for improvement in Ground Vibration Testing of large aircraft. In Proc. IFASD 2001 Int. Forum on Aeroelasticity and Struct. Dyn., Madrid, Jun 2001.," in *IFASD 2001 Int. Forum on Aeroelasticity and Struct. Dyn.*, Madrid, June 2001.

[6] P. Lubrina, "Ground vibration experiments on large civil aircraft for engine imbalance purpose," in *IFASD 2003 Int. Forum on Aeroelasticity and Struct. Dyn.*, Amsterdam, June 2003.

[7] H. Climent, "Aeroelastic and Structural Dynamics Tests at EADS CASA," in *the 18th Annual Symposium of the Society of Flight Test Engineers SFTE*, Madrid, June 2007.

[8] C.R. Pickrel, G.C. Foss, A. Phillips, R.J. Allemang, D.L. Brown, "New Concepts GVT," in *IMAC 24 Int. Modal Analysis Conf.,*, St. Louis (MO), , Jan-Feb 2006..

[9] H. Van Der Auweraer, D. Otte, J. Leuridan, W. Bakkers, "Modal testing with multiple sinusoidal excitation," in *IMAC 9 Int. Modal Analysis Conf.*, Firenze, 1991.

[10] D. Otte, H. Van Der Auweraer, J. Debille, J. Leuridan, "Enhanced force vector appropriation methods for normal mode testingm Los Angeles," in *February 1993*, Los Angeles, IMAC 11 Int. Modal Analysis Conf..

[11] L. Lauwers, J. Schoukens, R. Pintelon and M. Enqvist, "Nonlinear Structure Analysis Using the Best Linear," in *Proceedings of International Conference on Noise and Vibration Engineering*, Leuven, 2006.

[12] A. Esfahani, J. Schoukens and L. Vanbeylen, "Using the Best Linear Approximation With Varying Excitation Signals for Nonlinear System Characterization," *IEEE Transaction on Instrumentation and Measurement,* vol. 65, pp. 1271-1280, 2016.

[13] H. K. Wong, J. Schoukens and K. Godfrey, "Analysis of Best Linear Approximation of a Wiener–Hammerstein System for Arbitrary Amplitude Distributions," *IEEE Transactions on Instrumentation and Measurement,* vol. 61, no. 3, pp. 645-654, 2012.

[14] J. Schoukens and R. Pintelon, "Study of the Variance of Parametric Estimates of the Best Linear Approximation of Nonlinear Systems," *IEEE Transactions on Instrumentation and Measurement,* vol. 59, no. 12, pp. 3156-3167, 2010.

[15] Schoukens, J.; Vaes, M.; Pintelon, R., "Linear System Identification in a Nonlinear Setting. Nonparametric Analysis of the Nonlinear Distortions and Their Impact on The Best Linear Approximation.," *IEEE Control Systems Magazine,* vol. 36, pp. 38-69, 2016.

[16] T. Dobrowiecki, J. Schoukens, P. Guillaume, "Optimized excitation signals for MIMO frequency function measurements," *IEEE Transactions on Instrumentation and Measurements,*, vol. 55, pp. 2072-2079, 2006.

[17] T. Dobrowiecki and J. Schoukens, "Linear approximation of weakly nonlinear MIMO systems," *IEEE International Instrumentation and Measurement Technology Conference (I2MTC),* pp. 1607-1612, 2004.

[18] J. Schoukens, R. Pintelon, G. Vandersteen, Y. Rolain, "Design of excitation signals for nonparametric measurements on MIMO-systems in the presence of nonlinear distortions, IEEE International Instrumentation and Measurement Technology Conference," in *IEEE International Instrumentation and Measurement Technology Conference*, Austin, 2010.

[19] J. Schoukens, Y. Rolain, G. Simon, R. Pintelon, "Fully Automated Spectral Analysis of Periodic Signals," *IEEE Transactions on Instrumentation and Measurement,* vol. 52, no. 4, pp. 1021-1024, 2003.

[20] R. Pintelon, J. Schoukens, System Identification: A Frequency Domain Approach, 2nd ed., New Jersey: Wiley-IEEE Press, ISBN: 978-0470640371, 2012.

[21] L. Ljung, System identification: Theory for the User, 2nd ed., New Jersey: Prentice-Hall, ISBN: 9780136566953, 1999.

[22] P. Z. Csurcsia and J. Lataire, "Nonparametric Estimation of Time-variant Systems Using 2D Regularization," *IEEE Transactions on Instrumentation & Measurement,* vol. 65, no. 5, pp. 1259-1270, 2016.

[23] P. Z. Csurcsia, "Static nonlinearity handling using best linear approximation: An introduction," *Pollack Periodica* , vol. 8, no. 1, 2013.

[24] W. Heylen, P. Sas, Modal Analysis Theory and Testing, Leuven: Lirias, 2005.

[25] Kollár I, Pintelon R, Schoukens J, "Frequency Domain System Identification Toolbox for Matlab: A Complex Application Example.," in *IFAC International Symposium on System Identification and Parameter Estimation*, Copenhagen, 1997.

[26] Siemens, *Simcenter Testlab,* https://www.plm.automation.siemens.com/global/en/products/simcenter/.

[27] J. Schoukens, R. Pintelon, Y. Rolain, Mastering System Identification in 100 exercises, New Jersey: John Wiley & Sons, ISBN: 978047093698, 2012.

[28] J. Ortega Almirón, F. Bianciardi, P. Corbeels, W. Desmet, "Predicting vibration levels on an experimental test case by using invariant loads (e.g. Blocked forces) as source characterization," in *International Conference on Noise and Vibration Engineering* , Leuven, 2018.

[29] B. Cornelis, A. Toso, W. Verpoest, B. Peeters, "Improved MIMO FRF estimation and model updating for robust Time Waveform Replication on durability test rigs," in *International Conference on Noise and Vibration Engineering*, Leuven, 2014.

[30] M. Solomou and D. Rees, "Measuring the best linear approximation of systems suffering nonlinear distortions: An alternative method," *IEEE Transactions on Instrumentation and Measurements,* vol. 52, no. 4, pp. 1114-1119, 2003.

[31] T. Dobrowiecki and J. Schoukens, "Linear approximation of weakly nonlinear MIMO systems," *IEEE International Instrumentation and Measurement Technology Conference (I2MTC),* pp. 1607-1612, 2004.

[32] P. Guillaume, R. Pintelon, and J. Schoukens, "Accurate estimation of multivariable frequency response functions," *13th World Congress of IFAC,* vol. 29, no. 1, pp. 4351 - 4356, 1996.

[33] S. Petre, R. Moses, Spectral Analysis of Signals, New Jersey: Prentice Hall, 2005.

[34] J. Antoni, J. Schoukens, "Optimal Settings for Measuring Frequency Response Functions with Weighted Overlapped Segment Averaging," *IEEE Transactions on Instrumentation and Measurement,* vol. 58, no. 9, pp. 3276-3287, 2009.

[35] P. Z. Csurcsia, B. Peeters, J. Schoukens, "The Best Linear Approximation of MIMO Systems: First Results on Simplified Nonlinearity Assessment," in *IMAC International Modal Analysis Conference*, Orlando, 2019.

[36] T. McKelvey, G. Guérin, "Non-parametric frequency response estimation using a local rational model," in *IFAC Symposium on System Identification*, Brussels, 2012.

[37] R. Priemer, Introductory Signal Processing, World Scientific, ISBN: 9971509199, 1991.

[38] R. Pintelon, Y. Rolain, W. Van Moer, "Probability density function for frequency response function measurements using periodic signals," *IEEE Transactions on Instrumentation and Measurement,* vol. 52, no. 1, pp. 61-68, 2003.

[39] B. Peeters, M. El-Kafafy, P. Guillaume and H. Van der Auweraer, "Uncertainty propagation in Experimental Modal Analysis," in *Conference Proceedings of the Society for Experimental Mechanics Series*, 2014.

[40] P. Z. Csurcsia, B. Peeters, J. Schoukens, "The Best Linear Approximation of MIMO Systems: First Results on Simplified Nonlinearity Assessment," in *International Modal Analysis Conference*, Orlando, US, 2018.

[41] Wellstead P. E., "Non-parametric methods of system identification," *Automatica*, vol. 17, no. 1, pp. 55-69, 1981.

[42] Alvarez Blanco, M., Csurcsia, P. Z., Peeters, B., Janssens, K., Desmet, W., "Nonlinearity assessment of MIMO electroacoustic systems on direct field environmental acoustic testing," in *International conference on Noise and Vibration*, Leuven, Belgium, 2018.

[43] Alvarez Blanco, M., Csurcsia, P. Z., Carrera, A., Peeters, B., "Nonlinearity Assessment of MIMO Electroacoustic Systems," in *31st Aerospace Testing Seminar*, Los Angeles, USA, 2018.